Published in Palaeogeography, Palaeoclimatology, Palaeoecology 429 (2015) 83–99

Continental weathering and redox conditions during the early Toarcian Oceanic Anoxic Event in the northwestern Tethys: insight from the Posidonia Shale section in the Swiss Jura Mountains

Jean-Carlos Montero-Serrano [1,2,3,*], Karl B. Föllmi [1], Thierry Adatte [1], Jorge E. Spangenberg [1,4], Nicolas Tribovillard [5], Alicia Fantasia [1], Guillaume Suan [6]

[1] Institut des sciences de la Terre, Université de Lausanne, Bâtiment Géopolis, CH-1015 Lausanne, Switzerland

[2] Institut des sciences de la mer de Rimouski, Université du Québec à Rimouski, 310 allée des Ursulines, Rimouski, Quebec G5L 3A1, Canada

[3] Geotop Research Centre, Université du Québec à Montréal, Montréal, Quebec H3C 3P8, Canada

[4] Institut des dynamiques de la surface terrestre, Université de Lausanne, Bâtiment Géopolis, CH-1015 Lausanne, Switzerland

[5] Laboratoire Géosystèmes, UMR-8217, Université Lille 1, CNRS, Villeneuve d'Ascq, France

[6] UMR CNRS 5276 LGLTPE, Université Lyon 1, Campus de la Doua, Bâtiment Géode, F-69622 Villeurbanne Cedex, France

[*] Corresponding author: J.-C. Montero-Serrano. Phone: +1.418.723.1986 Ext: 1139; Fax: +1.418.724.1842; E-mail addresse: jeancarlos_monteroserrano@uqar.ca (J-C Montero-Serrano), karl.foellmi@unil.ch (K. Föllmi), Thierry.Adatte@unil.ch (T. Adatte), Jorge.Spangenberg@unil.ch (J. Spangenberg), Nicolas.Tribovillard@univ-lille1.fr (N. Tribovillard), Alicia.Fantasia@unil.ch (A. Fantasia), guillaume.suan@univ-lyon1.fr (G. Suan)

Highlights

-The T-OAE negative CIE reflects a ^{13}C-depleted carbon injection to ocean-atmosphere

-Detrital proxies suggest an increase in continental weathering rates during the T-OAE

-Redox proxies suggest moderate anoxic bottom-water conditions during the T-OAE

-Dysoxic-to-anoxic conditions prevailed until at least to the *bifrons* Zone

-P-enrichments are observed during the T-OAE

Abstract

The geochemistry and mineralogy of organic-rich sediments of the Rietheim succession in northern Switzerland were studied to evaluate the main impacts of the early Toarcian Oceanic Anoxic Event (T-OAE; ~183 Ma ago) on the depositional environment in the NW Tethys Ocean. The geochemical data obtained (notably, $\delta^{13}C_{org}$, $\delta^{13}C_{CaCO3}$, Rock-Eval pyrolysis, TOC_{cff}) support the hypothesis that the negative C-isotope excursion at the onset of the T-OAE mainly reflects a major perturbation in the global carbon cycle rather than local environmental changes (e.g., basinal restriction, productivity). Rock-Eval pyrolysis and $\delta^{13}C_{org}$-$\delta^{15}N_{total}$ crossplots indicate that the organic matter was primarily of marine origin during the T-OAE, and deposited in an epicontinental sea setting. Detrital proxies [notably, detritus index, siliciclastic balance and $Ln(Al_2O_3/Na_2O)$] suggest that the elevated pCO_2 levels and greenhouse climate prevailing during the T-OAE induced significant acceleration of the hydrologic cycle and an increase in continental chemical weathering rates. Redox-sensitive proxies [relative pyrite contents, organic and sulfide balances, V/(V+Ni) ratios, trace elements enrichment factors, trace-element-TOC co-variation patterns and TOC/P_{total} molar ratios] indicate that the Rietheim Posidonia Shale sediments accumulated under oxic-to-dysoxic bottom-water conditions, with more reducing conditions during the T-OAE (anoxic and possibly euxinic). These changes in redox conditions were probably induced by substantial thermohaline stratification driven by enhanced freshwater input and the recurrent influx of brackish Arctic seawater into the NW Tethys through the Viking Corridor, in agreement with previous sedimentological and geochemical evidences from the NW Tethys Ocean. In the studied succession, such conditions were perhaps also responsible for sequestration of most of the regenerated P in the deeper water column by adsorption and/or co-precipitation into authigenic phases. Overall, the major palaeoenvironmental changes documented in this study provide a robust example of Earth's possible responses to the rapid onset of extreme greenhouse conditions.

Keywords: Early Toarcian Oceanic Anoxic Event; Posidonia Shale; Geochemistry; Mineralogy; Paleoenvironment; Switzerland.

1. Introduction

The early Toarcian (~ 183 Ma ago) was a brief period in the Early Jurassic marked by an intense global warming to about 5–10°C warmer than at present (e.g., Chandler et al., 1992; Rosales et al., 2004; Dera et al., 2011). The lower Toarcian strata are characterized by a pronounced (4–7‰) near-global negative carbon isotope ($\delta^{13}C$) excursion recorded in organic matter, carbonates and fossil wood from open- and marginal-marine sections (e.g., Jenkyns et al., 2002; Hesselbo et al., 2007; Al-Suwaidi et al., 2010; Caruthers et al., 2011; Suan et al., 2011; Izumi et al., 2012; Reolid, 2014). It is currently thought that this intense global warming period and its associated environmental changes were the result of a major perturbation in the global carbon cycle, likely triggered by the combination of several geological processes, such as: (1) greenhouse gas inputs resulting from intensified rift-related tectonics (Bernoulli and Jenkyns, 2009) and large-scale eruptions in the Karoo-Ferrar large igneous province (Duncan et al., 1997; Pálfy and Smith, 2000), (2) thermogenic methane release related with magmatic intrusions and metamorphic alterations of Gondwanan coals and organic-rich shales in the Karoo-Ferrar province (e.g., Hesselbo et al., 2000; McElwain et al., 2005; Wignall et al., 2006; Svensen et al., 2007), (3) sudden dissociation of large amounts (~2500 Gt; Beerling and Brentnall, 2007) of continental-shelf methane hydrate deposits (e.g., Hesselbo et al., 2000; Kemp et al., 2005), possibly modulated by orbital forcing (Kemp et al., 2005, 2011). Note that thermogenic and biogenic methane are both powerful greenhouse gas enriched in isotopically-light carbon ($\delta^{13}C_{methane}$ < -60‰; e.g., Hesselbo et al., 2000), whereby a massive liberation of these gases may rapidly disrupt the global carbon cycle.

The extreme greenhouse conditions prevailing during early Toarcian also favoured a period of enhanced marine organic carbon deposition termed the early Toarcian Oceanic Anoxic Event or T-OAE

(e.g., Jenkyns, 1988; Baudin et al., 1990a). However, the expression of the early T-OAE has a wide geographic variability in terms of organic matter content and degree of oxygenation of bottom waters. Indeed, in many epicontinental sections from NW Europe and N Siberia (Fig. 1a), the T-OAE favoured a widespread deposition of organic-rich lithologies, such as black shales (e.g., Jenkyns, 1988; Baudin et al., 1990a,b; Hesselbo et al., 2000; Röhl et al., 2001; Cohen et al., 2004; Pearce et al., 2008; McArthur et al., 2008; Hermoso et al., 2009a,b; Suan et al., 2011). However, in more open marine sections from S Europe (Portugal - Suan et al., 2008; S Spain - Rodríguez-Tovar and Reolid, 2013), northern margin of Gondwana (Oman - Immenhauser et al., 1998; Morocco - Bodin et al., 2010; Algeria - Reolid et al., 2012, 2014a), as well as northern and southern Panthalassa Ocean (W Canada - Caruthers et al., 2011; NE Japan - Gröcke et al., 2011; NW Argentina - Al-Suwaidi et al., 2010), these organic-rich lithologies are absent or extremely condensed, suggesting that intensity of the T-OAE may have been strongly modulated by local and regional factors. In fact, as suggested in McArthur et al. (2008), the degree of water restriction and oxygen depletion varied regionally in Europe, increasing from South to North along the European Epicontinental Seaway. Overall, many of these studies quoted above have led to debate concerning the intensity of marine anoxia and geographic extent of the T-OAE.

In this context and in order to improve the characterization of the T-OAE within the NW Tethys Ocean, we present here a new high-resolution multi-proxy record [including the analysis of stable isotopes ($\delta^{13}C_{CaCO3}$, $\delta^{18}O_{CaCO3}$, $\delta^{13}C_{org}$, $\delta^{15}N_{total}$), bulk mineralogy, elemental geochemistry, and Rock-Eval pyrolysis] of an early Toarcian section located in the northern Swiss Jura Mountains (Rietheim village, Canton Aargau; Fig. 1). In this study, these new geochemical and mineralogical data have been used not only to explore the expression of the early T-OAE in an area not explored yet for its geochemistry, but also to better document the main impacts of this event on the depositional environment in the NW Tethys Ocean.

2. Geological setting

2.1. Depositional setting

During the Early to Middle Jurassic, the breakup of Pangaea led to the opening of the Central Atlantic and Tethys oceans (Fig. 1a), accompanied by widespread tectonic extension in what is now the Alpine-Mediterranean region, as well as in northern Europe (e.g., Bernoulli and Jenkyns, 2009). In western Europe, the early Toarcian is characterized by widespread organic-rich lithologies deposited in semi-restricted basins surrounded by shallow shelf seas extending across the West European platform to the northern Tethys Ocean (Fig. 1a; Jenkyns et al., 2002; Wignall et al., 2005; McArthur et al., 2008; Suan et al., 2008; Hermoso et al., 2009a,b, 2013). McArthur et al. (2008) suggested that water restriction varied regionally, being greatest in areas deeper and more distant from the Tethys Ocean (e.g., the Cleveland Basin; United Kingdom) and less restricted towards the south and east across the West European platform (e.g., the Paris Basin and SW Germany).

The Lower Jurassic stratigraphy in northern Switzerland (tabular and folded Jura; Fig. 1b) has been summarized recently by Reisdorf et al. (2011). The Early Jurassic Swiss deposits accumulated in the relatively slowly subsiding transition zone between the SW Germany Basin and the eastern Paris Basin under fully marine conditions (Reisdorf et al., 2011). Therefore, the lithology and fossil content of the Lower Jurassic deposits in northern Switzerland (such as the Posidonia Shale, renamed as Rietheim Member) are similar to those in SW Germany (e.g., Kuhn and Etter, 1994; Röhl et al., 2001; Röhl and Schmid-Röhl, 2005; Reisdorf et al., 2011).

2.2. Early Toarcian Posidonia Shale in northern Switzerland

The studied lower Toarcian Posidonia Shale is located in the Southern Tabular Jura, approximately 400 m SW of the village of Rietheim (Fig. 1b; Canton Aargau; 47°35’48.75’’N, 8°16’39.12’’E; cropping out in the bed of the Steigstrasse Stream). This Posidonia Shale succession

(~790 cm thick) has been lithostratigraphically and biostratigraphically well studied (Kuhn and Etter, 1994) including, in fact, three main ammonite biozones (*tenuicostatum*, *falciferum*, and *bifrons*) and several subzones (*exaratum*, *elegans*, *falciferum*, and *commune*) (Fig. 2). The transition between the *tenuicostatum* and *falciferum* zones is not precisely defined due to a scarcity of index fossils and/or to the presence of a stratigraphic gap in the Pliensbachian-Toarcian transition interval (Kuhn and Etter, 1994).

The bottom of the section, a glauconite-rich marl layer (~4 cm thick) and light-grey bioturbated marls, attributed to the *spinatum* Zone from the upper Pliensbachian, are intercalated with two compact marly-limestone beds about 10 and 18 cm thick, respectively (Fig. 2). The light-grey bioturbated marls contain diverse benthic micro- and macrofauna (including ammonites, belemnites and shell coatings) as well as phosphatic fish debris, disseminated framboidal pyrite, and pyritized fossils. The *tenuicostatum* Zone is represented by the transition of light-grey to dark-grey marly clays with generally low organic contents (<1%) and relatively abundant benthic fauna (notably bivalves and brachiopods). These marly clays (~ 30 cm thick) become more laminated and dark towards the upper part of the *tenuicostatum* Zone, where continuous organic-rich mudstone sedimentation started (up to the *bifrons* Zone). Indeed, black to brownish laminated bituminous marly clays ("Kartonschiefer-Fazies"; with more than 6% organic carbon) including fish and wood debris, pyritized ammonites, and disseminated framboidal pyrite prevail at the base of *falciferum* Zone. In contrast, weakly laminated black to grey bituminous marly clays ("Tonmergel-Fazies"; 1 to 6 wt.% organic carbon) dominate from the mid *falciferum* to the *bifrons* zones (Fig. 2). Silt-sized quartz grains are present in all types of laminations. Phosphate is commonly in the form of skeletal apatite at the base of *falciferum* Zone (as seen in thin sections; Kuhn and Etter 1994). Likewise, several thin bioturbated layers with moderately diverse benthic fauna occur within this bituminous marly-clayey facies. In fact, in comparison to the sediments at the base of *falciferum* Zone, the abundance of benthic fauna (e.g., *Pseudomytiloides dubius*) and trace fossils (e.g.,

Chondrites sp. and *Planolites* sp.) increases in the upper part of the section (*falciferum* to *commune* subzone).

The organic-rich mudstones are separated by several finely laminated limestone beds (Spinatumbank, Unterer Stein, Homogene Kalkbänke, Oberer Stein and Monotisbank) into a lower, middle, and upper part (Fig. 2). These limestone beds are likely of early diagenetic origin (Röhl et al., 2001; Röhl and Schmid-Röhl, 2005). The well-laminated limestone beds Unterer Stein and Oberer Stein can be traced over many kilometres within the epicontinental basin and are important marker beds (e.g., Kuhn and Etter 1994; Röhl et al., 2001). The micro-laminations are composed of alternating argillaceous, organic-rich, and fecal pellet/coccolith-rich layers (Kuhn and Etter 1994; Röhl et al., 2001). Finally, the top of the section (uppermost *commune* subzone) is marked by a 10–12 cm thick limestone bed (Monotisbank) with abundant shell debris (mainly the bivalve *Pseudomonotis substriata*) and ammonites (especially Dactylioceratidae).

3. Material and methods

3.1. Samples

The lower Toarcian Posidonia Shale succession of Rietheim was sampled systematically along the approximately 790 cm of the stratigraphic log (Fig. 2). A total of 226 samples were collected: 155 samples (vertical sample spacing, 2 cm) from a drill core in the first 316 cm of the stratigraphic log (Fig. 2), and 71 outcrop samples (vertical sample spacing, 5–10 cm) in the last 470 cm (Fig. 2). An aliquot (about 30 g) of each sample was crushed and pulverized using a Shatterbox with agate mills. Then, each sample was homogenized by sieving through a 100 mesh screen.

3.2. Analytical procedure

3.2.1. *Stable isotope analyses (carbon, oxygen, and nitrogen)*

Bulk carbonate carbon ($\delta^{13}C_{CaCO3}$) and oxygen ($\delta^{18}O_{CaCO3}$) isotope analyses were carried out on powdered bulk-rock samples using a Thermo Fisher Scientific GasBench II and carbonate preparation device interfaced to a Thermo Fisher Scientific Delta Plus XL continuous-flow isotope ratio mass spectrometer. Organic carbon ($\delta^{13}C_{org}$) and total nitrogen ($\delta^{15}N_{total}$) isotopes were also measured on the organic fraction of decarbonated (10% HCl treatment) samples using a Carlo Erba 1108 elemental analyser connected to a Thermo Fisher Scientific Delta Plus V isotope ratio mass spectrometer via a Confo III interface. The stable carbon and oxygen isotope ratios are reported in the delta notation as the per mil (‰) deviation relative to the Vienna Pee Dee Belemnite (VPDB) standard. The total nitrogen isotope ratios are also reported in the delta notation as the per mil (‰) deviation relative to atmospheric nitrogen (air N_2) standard. $\delta = [(R_{sample}/R_{standard}) - 1] \times 1000$ with $R={}^{13}C/{}^{12}C$, ${}^{18}O/{}^{16}$ and ${}^{15}N/{}^{14}N$. Analytical precision and accuracy were determined by replicate analyses and by comparison with international and in-house standards (Carrara marble, USGS-24, USGS-32, IAEA-N3, UREA, glycine, and pyridine), and were better than ±0.1‰ (1σ) for carbon, oxygen, and nitrogen.

3.2.2. *Rock-Eval pyrolysis*

The type and thermal maturity of the bulk organic matter (OM) was established by Rock-Eval pyrolysis using a model 6 device (Vinci Technologies) under standard conditions (see Béhar et al., 2001 for procedural details). The total organic carbon content (TOC, wt.%), T_{max} index (°C; OM thermal maturity indicators), Hydrogen Index (HI, mg HC/g TOC), and Oxygen Index (OI, mg CO_2/g TOC) were also determined. The HI and OI signatures allow a rough distinction between algal/bacterial (types I and II kerogen) and terrestrial plant (types III and IV kerogen) OM, as well as the degree of degradation and oxidation. Analytical precision was better than 0.05 wt.% (1σ) for TOC, 1.5°C (1σ) for Tmax, 10 mg HC/g TOC (1σ) for HI, and 10 mg CO_2/g TOC (1σ) for OI.

3.2.3. *Total organic carbon on the carbonate-free fraction*

In order to complement Rock-Eval data on the OM characteristics, we also quantified TOC concentrations on the carbonate-free fraction (cff) using a CHN Elemental Analyser (Carlo Erba Flash EA 1112 CHNS/MAS200). The decarbonated fraction was obtained by a double 10% HCl treatment. Precision was better than 1% based on an internal standard (methionine) and replicate samples. The TOC_{cff} allows a robust signature of the organic matter flux regardless of dilution due to carbonate input.

3.2.4. *Bulk-rock mineralogy*

The bulk-rock mineralogy was analysed by X-ray diffraction using a Thermo Scientific ARL X'TRA powder diffractometer. This instrument is fitted with a copper tube (Cu K-alpha = 1.540562Å), operating at 40 kV and 30 mA and a post-diffraction graphite monochromator. The random powdered rock samples were scanned from 2° to 65° two-theta in steps of 0.02° two-theta and a counting time of 1 second per step, resulting in 3151 data points. For the semi-quantification of the major mineralogical components, the bulk-rock XRD scans obtained were converted into mineral weight percents (wt.%) using the RockJock computer program (Eberl, 2003). This RockJock technique uses a full-pattern fitting method that permits the semi-quantification of whole-sediment mineralogy with a precision of 1-2%. To check the quality of this fitting procedure, a degree-of-fit (DOF = minimum absolute difference) statistic is calculated between the measured and simulated XRD patterns. The DOF obtained with our samples was good with values ranging from as low as 0.131 to as high as 0.402 and averaging 0.202 for the 187 samples. For this study the wt.% of the following minerals were calculated (Fig. 6): quartz, potassium (K) feldspar (microcline + orthoclase), plagioclase feldspar (albite), phyllosilicates (biotite, muscovite, illite, chlorite, and kaolinite), pyrite, dolomite, ankerite, and carbonate fluorapatite (CFA).

Because the quartz grains are principally detrital in the whole section (as seen in thin sections; Kuhn and Etter 1994), we determined a detritus index, calculated by summing quartz, phyllosilicates, K-feldspar, and Na-plagioclase contents, to observe changes in detrital influx (e.g., Keller et al., 2004; Westermann et al., 2010; Stein et al., 2012; Bomou et al., 2013). High detritus index values may indicate

higher delivery of terrigenous material from continental sources and/or decreased carbonate productivity and dissolution.

3.2.5. *Major, minor and trace element analysis*

Loss on ignition (LOI) was determined gravimetrically by heating the dried samples up to 1050°C for two hours. Major and trace-element concentrations were determined by X-ray fluorescence (XRF) spectrometry using a PANalytical PW2400 with an RX tube (Rh anode). Major (and minor) elements (Si, Ti, Al, Fe, Mn, Mg, Ca, Na, K, P) were measured after sample fusion with tetraborate, and trace elements (Nb, Y, Rb, Zn, Cu, Ni, Co, Cr, V, Nd, La, As) after mixing the samples with Mowiol polyvinyl alcohol (2%) and pressed to pellets. The detection limit for major elements is better than 0.01 wt.% and for trace elements is generally 1 to 4 ppm. Analytical reproducibility monitored by replicate analyses of selected samples was lower than ±5% for major, minor, and trace elements. Analysis accuracy was assessed by analyses of international and in-house standard reference materials (TS1-Cement, TS3-Clay, TS4-Limestone, TS5-Marlstone, TS7-Sandstone, 372-Portland cement, 368-Dolomite).

A compositional Q-mode cluster analysis (e.g., Egozcue and Pawlowsky-Glahn, 2005; Pawlowsky-Glahn and Egozcue, 2011) was performed on our elemental geochemical dataset with the goal of finding elemental associations with similar relative variation patterns that may be interpreted from a palaeoenvironmental standpoint (e.g., Jaminski et al., 1998; Hoffman et al., 1998; Reátegui et al., 2005; Montero-Serrano et al., 2010). This analysis was carried out using a log-ratio approach (Aitchison, 1986; Egozcue and Pawlowsky-Glahn 2005). Likewise, as measure of dissimilarity we use the variation array, and as clustering criterion the Ward method. Importantly, in order to isolate the siliciclastic component of the marls and marly clays, calcium-rich samples (Ca > 25 %, ~71 samples) are excluded from the Q-mode cluster analysis. All statistical calculations were conducted with “R” software using the

packages "StatDA" (Reimann et al., 2008) and "compositions" (van den Boogaart and Tolosana-Delgado, 2008).

In order to infer palaeoenvironmental changes (weathering, sediment supply, redox conditions) during the early T-OAE, the stratigraphic distribution of the elemental geochemical associations obtained by the compositional Q-mode cluster analysis were represented as elemental balances. Elemental balances are log-contrasts resulting from a log-ratio of two geometric means of two non-overlapping elemental groups (Egozcue and Pawlowsky-Glahn, 2005). The general expression of an elemental balance is:

$$b = [\sqrt{(r \times s / r + s)}] * \mathrm{Log}[gm(A)/gm(B)] \quad \textbf{[1]}$$

where A, B are two non-overlapping elemental groups of a complete composition x of D elements (e.g., Nb, Rb, La, K, Ti, Al, Si,…, x_D), r and s ($r + s \leq D$), are the number of elements in A, B respectively, and gm(.) denotes the geometric mean of the elemental groups A and B.

Alternatively, the chemical index of alteration (CIA), defined as: CIA = 100 × $Al_2O_3/(Al_2O_3 + CaO + Na_2O + K_2O)$ in molar proportions, may also be used as a proxy to the degree of weathering in the source areas with higher values suggesting more intense chemical weathering (Nesbitt and Young, 1982). However, samples that considerably vary in CaO due to presence of carbonate grains or cements (calcite or dolomite) and phosphates, such as samples studied here, may suggest misleading conclusions if the CIA is used to infer the degree of weathering (e.g., Cullers, 2000; Goldberg and Humayun, 2010). Under this context and based on a statistically model of linear compositional and weathering trends, von Eynatten et al. (2003) suggest that $Ln(Al_2O_3/Na_2O)$ (in molar proportions) may be used as a weathering index similar to CIA. Therefore, we prefer to use the $Ln(Al_2O_3/Na_2O)$ rather than CIA to infer changes in the degree of chemical weathering during deposition of the Rietheim Posidonia Shale succession. Using $Ln(Al_2O_3/Na_2O)$ has the advantage of avoiding uncertainties concerning the correction for CaO associated with phosphate and carbonate phases (e.g., Cullers, 2000; von Eynatten et al., 2003).

In addition, to compare the relative enrichment of redox-sensitive trace elements (RSTE: Cu, Ni, Zn, V, Co, As), we calculated Enrichment Factors (EF) by comparing Al-normalized metal concentration to those of average shale (Wedepohl, 1991): $X_{EF} = [(X/Al)_{sample} / (X/Al)_{average\ shale}]$. In practical terms, EF > 3 represents a detectable authigenic enrichment of an element over average shale concentrations, whereas EF > 10 represents a moderate to strong degree of authigenic enrichment (e.g., Tribovillard et al., 2006; Algeo and Tribovillard, 2009).

All analytical data presented are available electronically in the Supplementary Appendix A.

4. Results

4.1. Stable isotopes

Carbon isotope values of bulk OM ($\delta^{13}C_{org}$ ~ -32.6 to -25.3‰; Fig. 3a) and the carbonate ($\delta^{13}C_{CaCO3}$ ~ 1.2 to -2.6‰; Fig. 3b) of marls and marly clays show comparable variations throughout the section, with a pronounced negative carbon isotope excursion (or CIE) within the *exaratum* subzone (Fig. 3a-b). The magnitude of this negative CIE varies from ~3‰ in $\delta^{13}C_{CaCO3}$ to ~5‰ in $\delta^{13}C_{org}$ records. On average, the $\delta^{13}C_{org}$ values are in the range of $\delta^{13}C_{org}$ records of marine OM deposited during pronounced greenhouse phases (e.g., Dean et al., 1986; Jenkyns, 2010), whereas $\delta^{13}C_{CaCO3}$ values are within the range of early Toarcian $\delta^{13}C_{CaCO3}$ records from epicontinental seas of the Peritethyan Realm (e.g., Röhl and Schmid-Röhl, 2005; van de Schootbrugge et al., 2005; Hesselbo et al., 2007; Suan et la., 2008; Hermoso et al., 2009b).

Extremely light $\delta^{13}C_{CaCO3}$ values are found within limestone beds and bioturbated marls (e.g., -4.57‰ in the Unterer Stein; Fig. 3b). $\delta^{13}C_{org}$ and $\delta^{13}C_{CaCO3}$ values decrease slightly up section. Oxygen-isotope values of the bulk carbonate ($\delta^{18}O_{CaCO3}$) shows higher values in the upper Pliensbachian interval (-6 to -2.7‰) compared to the lower Toarcian (-8 to -7‰) (Fig. 3c). However, in the Spinatumbank, Unterer Stein, and Homogene Kalkbänke limestone beds, the $\delta^{18}O_{CaCO3}$ values are significantly higher (-

4 to -2.7‰). Nitrogen-isotope values of OM ($\delta^{15}N_{total}$) range between +1 and +3‰ throughout the section (Fig. 3d), with lower values (~ +0.4‰) in the limestone bed Unterer Stein. These $\delta^{15}N_{total}$ values are within the range of values that characterized the Jurassic-Cretaceous interval (Algeo et al., 2014).

4.2. Organic matter characterization

Total organic carbon (TOC), total organic carbon from the carbonate-free fraction (TOC_{cff}), and the hydrogen index (HI) show lower values (TOC < 0.5 wt.%; TOC_{cff} < 2 wt.%; HI < 70 mg HC/g TOC) in the upper Pliensbachian interval compared to the lower Toarcian (Fig. 3e-g), whereas oxygen index (OI) show higher values (up to 422 mg CO_2/g TOC; Fig. 4a). In fact, in the lower Toarcian interval, TOC, TOC_{cff}, HI and OI values range from 2 to 11.8 wt.%, 5 to 18 wt.%, 400 to 794 mg HC/g TOC, 49 to 422 mg CO_2/g TOC, respectively. High TOC (6 to 11.8 wt.%) and HI (600 to 794 mg HC/g TOC) as well as low OI (<10 mg CO_2/g TOC) values characterize the black to brownish laminated bituminous marly clays (*exaratum* subzone) recording the early Toarcian CIE, whereas lower TOC (< 2 wt.%) and HI (HI < 360 mg HC/g TOC) values characterize the early-diagenetic limestone beds as well as the bioturbated marl intervals. Rock-Eval T_{max} values average 427°C without any significant variation (Fig. 3h).

4.3. Bulk mineralogical composition

The bulk mineralogy in the Rietheim Posidonia Shale is dominated by calcite, phyllosilicates, and quartz, and lower proportions of K-feldspar, Na-plagioclase, pyrite, ankerite, dolomite, and carbonate fluorapatite or CFA (Fig. 6 and 7). An unidentified group of organic material and some poorly crystallized minerals (e.g., iron oxide) are unquantified and not considered here (Fig. 7j). In general, calcite distribution is inversely correlated to phyllosilicates, quartz, K-feldspar and Na-plagioclase (Fig. 7a-e). Calcite is the dominant mineral (60–96%) from the finely laminated limestone beds (e.g., Unterer Stein, Homogene Kalkbänke, Oberer Stein, and Monotisbank), whereas phyllosilicates (19–53%) and quartz (5–18%) are the dominant minerals in the marl and marly clay intervals (Fig. 7a-e). A decrease in

calcite content from 60% to 25% is observed at the base of the *exaratum* subzone (Fig. 7e). The upper Pliensbachian (*spinatum* Zone) interval is characterized by high ankerite (up to 18%) and dolomite (up to 7.5%) contents (Fig. 7f-g). Indeed, the vertical distribution of dolomite mimics the ankerite record. The CFA ranges between 0% to 1.6%, with higher values at the base of *falciferum* and *bifrons* zones (Fig. 7h). The pyrite content increases (up to 6.9%) in *exaratum* subzone (broadly coeval with the negative CIE) and then slowly decrease upsection (Fig. 7i).

4.4. Major, minor and trace element analysis

The compositional Q-mode cluster analysis of the Rietheim Posidonia Shale succession samples revealed three major elemental geochemical associations (Fig. 8):

(1) Siliciclastics (Nb, Rb, La, K, Ti, Al, Si, Cr, Na, Y, Nd, Mg): this geochemical group consists of elements associated with clay and silt particles, mainly as chemical constituents of the detrital mineral grains (e.g., phyllosilicates, quartz, Na-plagioclases, K-feldspar) or adsorbed on their surface (e.g., Calvert and Pedersen, 2007; Montero-Serrano et al., 2010). However, Mg shows a different vertical distribution with respect to the other siliciclastics elements (Fig. 8a), likely suggesting that this element is also associated with dolomite and ankerite (Fig. 7f-g). Overall, the variability of riverine and aeolian inputs related to continental climatic fluctuations as well as the hydraulic partitioning of the sediments mostly control the distribution and accumulation of these elements.

(2) Organic (P, As, TOC, Ni, V) – sulfide (Zn, Cu, Fe, Co): these elements are commonly associated with the OM and the authigenic sulfides (e.g., pyrite) fraction, whose accumulation is largely controlled by the oxic-anoxic conditions of the sedimentary environment (e.g., Jaminski et al., 1998; Algeo and Maynard, 2004; Tribovillard et al., 2006; Calvert and Pedersen, 2007). Among these elements, V/(V+Ni) ratio and TOC/P_{total} molar ratios are reputed as paleoredox-indices (e.g., Hatch and Leventhal, 1992; Jones and Manning, 1994; Algeo and Maynard, 2004;

Tribovillard et al., 2006; Algeo and Ingall, 2007). Indeed, V/(V+Ni) ratios lower than <0.46, 0.46–0.60, 0.54–0.82, greater than 0.82 may suggest oxic, dysoxic, anoxic and euxinic conditions in the water column., respectively (Hatch and Leventhal, 1992).

(3) Carbonates (Ca, Mn): this geochemical group consists of elements related with calcium carbonate (mainly calcite) associated with calcareous cement as well as benthic fauna (including ammonites, belemnites, shell coatings) and coccoliths, which agrees with the petrographic interpretations (Kuhn and Etter 1994). The carbonate-associated elements correlate negatively with the other two elemental associations, and thus likely represent a dilution fraction.

Based on these geochemical associations, elemental balances are performed (e.g., $b_{\{siliciclastic/carbonate\}}$, $b_{\{sulphide/carbonate\}}$ and $b_{\{organic/carbonate\}}$). The vertical distribution of siliciclastic (Nb-Rb-La-K-Ti-Al-Si-Cr-Na-Y-Nd), sulfide (Fe-Cu-Zn-Co) and organic (TOC-P-As-V-Ni) balances show similar patterns across the Rietheim Posidonia Shale succession (Fig. 8a-d; Fig. 10c; Fig. 11b-c), with minimum values recorded in the *spinatum* Zone and maximum values in the negative CIE (*exaratum* subzone) that then slowly decrease upsection. Similarly, $Ln(Al_2O_3/Na_2O)$ values also increase significantly during the negative CIE (*exaratum* subzone), then slowly decrease upsection and increasing again during the upper part of *commune* subzone (Fig. 10b). The V/(V+Ni) ratio range between 0.50 to 0.85 with maximum values recorded also during the negative CIE that then slowly decrease upsection (Fig. 11d). RSTE enrichment factors (Cu, Ni, Zn, V, Co, As) show a modest enrichment (2 to 9) within the negative CIE compared to average shale values (Fig. 11e-f). Finally, a good correspondence is observed between the different detrital [detritus index, siliciclastic balance, $Ln(Al_2O_3/Na_2O)$; Fig. 10] and redox [pyrite content, sulfide and organic balances, V/(V+Ni); Fig. 11a-f, i] proxies used here.

4.5. Phosphorus contents and TOC/P_{total} molar ratios

In the Rietheim succession, profiles of total P contents mimic the stratigraphic trend of the CFA, with higher values during the negative CIE and early *bifrons* Zone (Figs. 8d and 11g). Furthermore,

higher P values correspond also to higher TOC values during the negative CIE (Fig. 8d), whereas lower total P contents are characterized in the upper part of *exaratum* and at the base of *elegans* subzones.

We also determined C_{org}/P_{org} molar ratios to evaluate the burial efficiency of P relative to total organic-matter preservation in the sediments (e.g., Algeo and Ingall, 2007; Westermann et al., 2013). Indeed, C_{org}/P_{org} molar ratios measured in organic-rich sediments may reflect the importance of preferential P release under dysoxic-to-anoxic bottom-water conditions and as such serve as a paleoredox proxy (e.g., Bodin et al., 2006; Algeo and Ingall, 2007; Mort et al., 2007; Bodin et al., 2010; Stein et al., 2011; Westermann et al., 2013). In this study, we use TOC/P_{total} molar ratios ($P_{total} = P_{reactive} + P_{detritic}$; assuming the $P_{detritic}$ is likely to represent well-crystallized authigenic carbonate fluorapatite) rather than C_{org}/P_{org} or $C_{org}/P_{reactive}$ ($P_{reactive} = P_{oxide\text{-}associated} + P_{authigenic} + P_{org}$; Anderson and Delaney, 2001), since as discussed in Algeo and Ingall (2007), the $P_{detritic}$ is generally a minor component (mean ~13%) of P_{total} in black shales units. This assumption is in agreement with the compositional Q-mode cluster analysis, where P_{total} is associated with TOC (Fig. 8d-e). The TOC/P_{total} molar ratios calculated for the Rietheim Posidonia Shale succession range from 37 to 383 (median ~ 167) at the base of *falciferum* Zone, with maximum values within the upper part of the *exaratum* subzone (Fig. 11h). Conversely, in the *spinatum*, upper part of the *falciferum* and base of *commune* subzones, TOC/P_{total} molar ratios are lower, ranging from 33 to 160 (median ~ 78). In general, the increases in the TOC/P_{total} molar ratios are associated to relatively low P concentrations (Fig. 8d) and CFA contents (Fig. 11g).

5. Interpretation and discussion

5.1. Diagenetic effects

The anomalous $\delta^{13}C_{CaCO3}$ and $\delta^{18}O_{CaCO3}$ values observed within limestone beds and bioturbated marls in the Rietheim Posidonia Shale succession likely reflect early diagenetic carbonate precipitation (e.g., Algeo et al., 1992; Röhl and Schmid-Röhl, 2005). Therefore, in order to improve the

palaeoenvironmental signature of our geochemical records, these limestone beds and bioturbated marls (~ 71 samples of the global geochemical dataset) were excluded from the subsequent interpretation and discussion.

Stable oxygen isotopes in carbonates are more affected by diagenesis compared to carbon isotopes (Schrag et al., 1995). At the Rietheim Posidonia Shale succession, the observed $\delta^{18}O_{CaCO3}$ pattern (higher values in limestone beds and lower in marls; Fig. 3c) most likely reflects the timing of burial diagenesis, rather than changes in the palaeoceanic isotope signal (such as salinity and temperature). Indeed, during burial diagenesis, limestone cement forms early, in shallow depths and lower burial temperatures, and thus acquires higher $\delta^{18}O$ values (-5 to -2‰) compared to marls (-9 to -6‰), which cement later (e.g., Algeo et al., 1992; Schrag et al., 1995; Rosales et al., 2001).

In this context and despite the diagenetic alteration of the $\delta^{18}O_{CaCO3}$ signature, the $\delta^{13}C_{CaCO3}$ as well as the $\delta^{13}C_{org}$ records probably represent a mainly palaeoenvironmental origin because they are in the same range of values and have similar rates of changes to those found in the Tethys, subboreal and Proto-Atlantic Oceans (e.g., Jenkyns, 1988; Hesselbo and Jenkyns, 1998; Hesselbo et al., 2000; Röhl et al., 2001; Röhl and Schmid-Röhl, 2005; Suan et al., 2008; Hermoso et al., 2009a,b; and references therein).

5.2. Maturity, sources and preservation of the organic matter

Rock-Eval T_{max} values average 427°C without any significant variation, indicating that the OM in the Rietheim Posidonia Shale succession is immature with regards to hydrocarbon generation (Fig. 3h). Therefore, variations in HI and OI cannot be attributed to changes in thermal maturity. The sudden shifts towards lower HI values (<450 mg HC/g TOC) observed through the lower Toarcian interval (e.g., in the thin bioturbated horizons between the *falciferum* and *commune* subzones; Fig. 3g and Fig. 4a) likely suggest enhanced OM degradation during intermittent periods of oxygenation (e.g., Röhl and Schmid-Röhl, 2005). The vertical distribution of HI (Fig. 3g) together with HI-OI crossplots (Fig. 4a) indicate

that OM in the upper Pliensbachian interval mainly consists of recycled and/or terrestrial material (type III/IV kerogen), whereas in the lower Toarcian interval, it is mainly dominated by marine phytoplankton and algal material (type I/II kerogen). Similar OM characteristics have also been reported in nearby lower Toarcian successions from SW Germany (e.g., Röhl et al., 2001; Röhl and Schmid-Röhl, 2005).

The $\delta^{13}C_{org}$-$\delta^{15}N_{total}$ crossplots (Algeo et al., 2014) suggest that the Rietheim Posidonia Shale succession was deposited in an open epicontinental sea setting (Fig. 4c). In this depositional setting the variability in sedimentary dynamics might have been driven by fluctuations in sea level (Reisdorf et al., 2011). Indeed, sequence stratigraphic studies from NW Tethys have provided evidence for sea-level fall close to the onset of the early Toarcian negative CIE (e.g., Perilli, 2000; Wignall et al., 2005; Pittet et al., 2014). Accordingly, the OM source changes observed in the Rietheim Posidonia Shale succession may have been related to eustatic sea-level changes. A sea-level lowstand during the upper Pliensbachian interval may explain the increase in terrestrial-derived OM, whereas the enhanced input of marine-derived OM in the lower Toarcian interval may correspond to a rising sea-level trend. Likewise, the relatively high TOC (up to 11.8 wt.%) and TOC_{cff} (up to 18 wt.%) recorded in the lower Toarcian interval (Fig. 3e-f) suggests that likely elevated surface productivity and/or oxygen-depleted bottom-water conditions prevailed in the NW Tethys during the T-OAE. These depositional conditions were very favourable to OM preservation in the Rietheim Posidonia Shale succession. Similar results have been reported by Röhl et al. (2001) and Röhl and Schmid-Röhl (2005) in the Posidonia Shale succession from SW Germany.

5.3. Link between organic matter source and organic carbon isotopes

The larger amplitude of the negative CIE observed in $\delta^{13}C_{org}$ records relative to $\delta^{13}C_{CaCO3}$ in the Rietheim Posidonia Shale might be related by changes in OM sourcing (e.g., van de Schootbrugge et al., 2013). The influence of changes in the type of preserved OM on the $\delta^{13}C_{org}$ records may be explored by comparing pre- and post-excursion $\delta^{13}C_{org}$ values with coeval HI values (e.g., van de Schootbrugge et

al., 2013). In the Rietheim Posidonia Shale succession, $\delta^{13}C_{org}$-HI crossplots data from the *spinatum* and *bifrons* zones show a significant negative correlation (Fig. 4b), suggesting that part of the bulk $\delta^{13}C_{org}$ records likely reflect changes in OM sourcing. Following the approach proposed by van de Schootbrugge et al. (2013), the residual changes that are not explained by HI variations may be calculated by subtracting the $\delta^{13}C_{org}$ values reconstructed from the $\delta^{13}C_{org}$-HI crossplots from the $\delta^{13}C_{org}$ data. For the studied succession, the obtained residual $\delta^{13}C_{org}$ record (hereinafter $\delta^{13}C_{org\ HI\text{-}corr}$) show an overall shape and negative CIE magnitude (~ 3‰) similar to the bulk $\delta^{13}C_{CaCO3}$ record (Fig. 5b-c). These results support the idea that the raw $\delta^{13}C_{org}$ records cannot be used for reconstructing global carbon cycle perturbations without careful consideration of the OM sources (van de Schootbrugge et al. 2013).

5.2. Palaeoenvironmental changes related to the Toarcian Oceanic Anoxic Event

The variations observed in the mineralogical and geochemical record of the Rietheim Posidonia Shale section are likely related to the onset of the T-OAE during the Early Jurassic. Hence, we discuss our results in terms of the major palaeoenvironmental changes, which fostered deposition of the Rietheim Posidonia Shale in the NW Tethys Ocean during the early T-OAE.

5.2.1. *Origin of the negative $\delta^{13}C$ excursion and global carbon cycle perturbations*

$\delta^{13}C_{org\ HI\text{-}corr}$ and $\delta^{13}C_{CaCO3}$ records of marls and marly clays show a parallel temporal evolution throughout the Rietheim Posidonia Shale succession, with a pronounced negative CIE (~ 3‰) within the *exaratum* subzone (Fig. 5). This parallel trend, together with the magnitude of the negative CIE, supports the hypothesis that the early Toarcian negative CIE mainly reflects a major perturbation in the global carbon cycle, likely associated both with an massive output of volcanogenic CO_2 and thermogenic methane (CH_4) from OM sources in the Karoo-Ferrar large igneous province (e.g., Hesselbo et al., 2000; Svensen et al., 2007; Hesselbo et al., 2007; Suan et al., 2008).

However, the magnitude of this negative CIE in the Rietheim Posidonia Shale succession is slightly reduced (~3‰) compared, for example, to lower Toarcian strata from SW Germany

(Dotternhausen; Röhl and Schmid-Röhl, 2005), the UK (Yorkshire; Hesselbo et al., 2000; Kemp et al., 2005), and northern Siberia (Kelimyar River; Suan et al., 2011) (Fig. 9). In agreement with Kuhn and Etter (1994) and Reisdorf et al. (2011), we attribute this to the presence of a stratigraphic gap in the Pliensbachian-Toarcian transition interval. Indeed, most of the *tenuicostatum* Zone, where $\delta^{13}C_{org}$ values up to -26‰ are frequently recorded (Röhl and Schmid-Röhl, 2005; Fig. 9b), is missing in the Rietheim Posidonia Shale succession (Kuhn and Etter, 1994). This interpretation is supported by the fact that $\delta^{13}C_{org}$ values recorded just below the limestone bed Unterer Stein in Dotternhausen (Röhl et al., 2001; Röhl and Schmid-Röhl, 2005) and Rietheim are almost identical (~ -32.6‰; Fig. 9a-b). Similar interpretations have also been performed by Röhl and Schmid-Röhl (2005) in the Franconian Posidonia Shale succession from Schesslitz in SW Germany, as well as by Pittet et al. (2014) in the Lusitanian Basin (Portugal) and Ruebsam et al. (2014) in the Lorraine Sub-Basin (NE Paris Basin, France). Therefore, we hypothesize that lower Toarcian strata deposited in a basin-margin setting, such as the Rietheim in northern Switzerland, were probably affected by processes of submarine erosion, reworking, and/or non-deposition due to a fast drop in relative sea-level during the Pliensbachian–Toarcian transition (e.g., Kuhn and Etter, 1994; Hardenbol et al., 1998; Röhl and Schmid-Röhl, 2005; Reisdorf et al., 2011; Pittet et al., 2014; Ruebsam et al., 2014).

5.2.3. *Continental weathering*

Changes in the weathering at the source areas and clastic influx that prevailed during deposition of the Rietheim Posidonia Shale succession can be inferred using the mineralogical and geochemical data here obtained (Fig. 10). Indeed, the detritus index, siliciclastic balance and $Ln(Al_2O_3/Na_2O)$ are based on minerals (quartz, phyllosilicates, K-feldspar, Na-plagioclase) and chemical elements, which mainly constitute the detrital component (Nb-Rb-La-K-Ti-Al-Si-Cr-Na-Y-Nd). Consequently, higher values in these detrital proxies could be interpreted here as periods of: (1) stronger rainfall, enhanced chemical weathering and continental runoff, and/or (2) lowered carbonate production in surface water.

In the Rietheim Posidonia Shale succession, the meaningful increase in the detritus index, siliciclastic balance and Ln(Al_2O_3/Na_2O) observed during the early Toarcian negative CIE (*exaratum* subzone; Fig. 10) suggest a greater increase in detrital input during this interval relative to the rest of the succession, likely due to an enhanced terrestrial discharge resulting from a strongly accelerated hydrological cycle and higher continental weathering rates induced by intensification of greenhouse conditions during the early T-OAE. Seawater osmium-isotope excursion to more radiogenic values (Cohen et al., 2004) in the NW Tethys Ocean also suggest a warm and humid climate as well as a transient increase in continental weathering rates during the early T-OAE. Likewise, numerical models on regional hydrologic responses to large-scale atmospheric circulation patterns during the Early Jurassic indicate that strong monsoonal circulation dominated along the mid-latitude coasts of Tethys and Panthalassa during the Early Jurassic, including the early Toarcian (e.g., Parrish and Curtis, 1982; Chandler et al., 1992; Dera and Donnadieu, 2012). These monsoonal systems are likely associated with localized pressure cells whose positions are controlled by topography and coastal geography (Chandler et al., 1992). In fact, the large continental areas were mainly located between 30° and 60° latitude in both hemispheres during the Early Jurassic (Fig. 1a), which led to a meridional trade-wind/monsoon-wind circulation pattern (e.g., Parrish and Curtis, 1982; Chandler et al., 1992; Röhl et al., 2001).

However, the increase in the detritus index and siliciclastic balance during the negative CIE likely cannot be entirely attributed to a strongly enhanced detrital discharge. The pronounced decrease in both calcite (from 60% down to 14%; Fig. 7e) and Ca (from 20 down to 5%; Fig. 8b) contents at the onset of the negative CIE instead suggest that the increase in these proxies may also reflect a relative decrease in carbonate productivity. Thus, in agreement with several studies on continental weathering, carbonate production and ocean acidification during the early Toarcian (e.g., Röhl et al., 2001; Cohen et al., 2004; Suan et al., 2008; Mattioli et al., 2008, 2009; Hermoso et al., 2009a,b; Dera et al., 2009; Trecalli et al., 2012; Hermoso and Pellenard, 2014; Reolid et al., 2014b), we hypothesize that this drop

in carbonate content recorded at the onset of the negative CIE in the Rietheim Posidonia Shale succession (Fig. 8b) may likely be the result of a combination of three main factors: (1) dilution by higher detrital input resulting from an accelerated hydrological cycle and enhanced continental runoff, (2) decreasing in carbonate production associated with an enhanced continental runoff and southwards flux of brackish Arctic seawater which controlled turbidity and salinity in surface waters within the NW Tethys Ocean, and/or (3) enhanced carbonate dissolution related to strong seawater acidification conditions driven by a massive injection of CO_2 into the atmosphere and then into the ocean.

Overall, our mineralogical and geochemical proxies support the hypothesis that the massive injection of CH_4/CO_2 into the ocean-atmosphere system and subsequent global warming induced during the Early T-OAE an acceleration of the hydrologic cycle and an increase in global chemical weathering rates as well as possibly also decreasing in carbonate production (e.g., Mattioli et al., 2009; Trecalli et al., 2012). However, further investigations are required to improve this latter hypothesis in the Rietheim Posidonia Shale section.

5.2.4. *Redox conditions*

In this study, redox conditions that prevailed during the deposition of the Rietheim Posidonia Shale succession are investigated using several proxies (Fig. 11a-f and Fig. 12): pyrite content, sulfide (Fe-Cu-Zn-Co) and organic (TOC-P-As-V-Ni) balances, the V/(V+Ni) ratio, RSTE enrichment factors, relationships between Al-normalized RSTE and TOC and the TOC/P_{total} molar ratios.

-Inferences from pyrite, redox-sensitive elements and V/(V+Ni) ratio

The stratigraphic distribution of relative contents of pyrite (%), sulfide (Fe-Cu-Zn-Co) and organic components (TOC-P-As-V-Ni) as well the V/(V+Ni) ratio show similar trends across the Rietheim Posidonia Shale succession, with higher values recorded during the negative CIE (*exaratum* subzone) that then slowly decrease upsection (Fig. 11a-d). These stratigraphic trends, together with threshold values proposed by Hatch and Leventhal (1992) for the V/(V+Ni) ratio (see Section 4.4),

suggest that sediments in the *exaratum* subzone represent the onset as well as peak of the T-OAE episode where anoxic (and possibly euxinic) conditions prevailed at the sediment-water interface, whereas the remainder of the *falciferum* Zone and the overlying *bifrons* Zone represent a continuation of oxic-to-dysoxic conditions. The modest enrichment (2 to 9), which exhibit the RSTE (Cu, Ni, Zn, V, Co, As) compared to average shale values within the negative CIE also supports the interpretation that anoxic bottom-water conditions developed during the *exaratum* subzone (Fig. 11e-f). Similar results have been obtained by Brumsack (1991) in the nearby Posidonia Shale succession from the SW Germany.

The redox conditions, which prevailed in the sedimentary environment, can also be inferred through the co-variation patterns between the Al-normalized RSTE and TOC (Fig. 12a; Algeo and Maynard, 2004; Tribovillard et al., 2006). Note in Fig. 12 that Al-normalized RSTE (V, Ni, As and Cu) plotted versus TOC allows the discrimination of different redox facies (dysoxic, anoxic and euxinic) in both modern (Irino and Pedersen, 2000; Tada et al., 2000; Piper and Dean, 2002) and ancient (Arthur et al., 1990; Brumsack, 1991; Warning and Brumsack, 2000; Algeo and Maynard, 2004) marine depositional environments. In the Rietheim Posidonia Shale succession, these Al-normalized RSTE-TOC co-variation patterns (Fig. 12b-e) suggest that the predominating palaeo-oxygenation conditions during the deposition of these sediments were (1) oxic during the *spinatum* subzone, (2) anoxic (possibly euxinic) during the *exaratum* subzone, and (3) dysoxic, with intermittent anoxia, during the *elegans* to *commune* subzones.

Based on the similar covariation between the detritus index, siliciclastics, organic and sulfide balances during the negative CIE (Fig. 10), we hypothesize that detrital inputs may indirectly represent the main cause for the modest excess of trace-metal content in the *exaratum* subzone. Indeed, in marginal environments, enhanced continental runoff during the early T-OAE likely provided high amounts of nutrients, which lead to increased productivity and greater settling of OM. In addition,

according to Mattioli et al. (2009) and Dera and Donnadieu (2012), enhanced freshwater input in conjunction with the recurrent influx of brackish Arctic seawater through the Viking Corridor could have increased the themohaline stratification within the NW Tethys Ocean during the early T-OAE. Overall, the combined effects of these processes likely induced depletion in bottom-water oxygen levels and thus a modest RSTE enrichment. Consequently, from a geochemical point of view, the organic-rich sediments of the *exaratum* subzone were likely deposited in a sedimentary environment very similar to the more recent Plio-Pleistocene Black Sea and/or Mediterranean sapropels (e.g., Brumsack, 1991). That is, a stratification of the water column due to salinity differences and the prevalence of anoxic to euxinic bottom-water conditions (e.g., Murray et al., 1989; Brumsack, 1991).

-*Inferences from phosphorus contents and TOC/P_{total} molar ratios*

P is an important limiting nutrient in the ocean, driving primary productivity (e.g., Tyrrell, 1999; Benitez-Nelson, 2000). The flux of dissolved P into the ocean is mainly controlled by continental runoff (Föllmi, 1996), and the transfer of P into sediments occurs by incorporation into OM and fish debris or by aggregation onto clay particles, iron, and manganese oxyhydroxides (Delaney, 1998). However, P burial within sediments is strongly influenced by changes in the benthic redox conditions (e.g., van Cappellen and Ingall, 1994; Ingall et al., 2005; Algeo and Ingall, 2007; Mort et al., 2007). Indeed, dysoxic-to-anoxic bottom-water conditions not only promote an enhanced preservation of OM but also a remobilization and release of mineral-associated phosphate and organic P into the uppermost sediments and overlying water column (van Cappellen and Ingall, 1994; Ingall et al., 2005; Mort et al., 2007). Under such conditions, the increased regeneration of P in sediments may lead to both enhanced phosphate recycling (low P burial efficiency) and increased primary productivity in a positive feedback loop (van Cappellen and Ingall, 1994; Ingall et al., 2005), resulting in sedimentary C_{org}/P_{org} ratios higher than the Redfield ratio of 106 (Redfield, 1958, Algeo and Ingall, 2007).

In Rietheim Posidonia Shale succession, TOC/P_{total} molar ratios higher than the Redfield ratio (106 to 383; Fig. 11h) at the base of *falciferum* Zone suggest that the deposition of organic-rich sediments during the early Toarcian may have occurred under more oxygen-depleted conditions. These interpretations are in agreement with the stratigraphic trends of all RSTE proxies (Fig. 11a-f and Fig. 12), which suggested a moderate shift toward anoxic conditions. Conversely, TOC/P_{total} molar ratios lower than the Redfield ratio (<106) associated to relatively high P and CFA contents in the *spinatum*, upper part of the *falciferum* and base of *commune* subzones suggest that the depositional environment evolved towards more oxic-to-dysoxic bottom waters. Note that the presence of oxygen not only promotes the oxidative destruction of OM but also retention of remineralized organic P within the sediment (Algeo and Ingall, 2007). The predominance of bioturbated layers in the upper part of the Rietheim Posidonia Shale succession supports this interpretation (Fig. 2). However, because high P and CFA contents are not coincident with maxima in TOC content in the *spinatum*, upper part of the *falciferum* and base of *commune* subzones, these P-rich intervals might also be related with a high abundance of preserved fish debris within the sediment (see Section 2.2). Large amount of fish debris have also been reported in the *falciferum-bifrons* Zone boundary from lower Toarcian sections of the SW Germany (Rohl and Schmid-Rohl, 2005) and SE France (Suan et al., 2013).

On the other hand, the high P contents associated with the high TOC values during the negative CIE (Fig. 8d) suggest that a part of the remobilized P during redox recycling was likely trapped within the sediments in authigenic P bearing minerals (e.g., authigenic apatite). Indeed, we hypothesize that oxygen-depleted bottom-water condition in conjunction with enhanced surface water stratification led to sequestration of a large part of the regenerated P in the deeper water column by adsorption and/or co-precipitation into authigenic phases (e.g., apatite). This has also been observed in Mediterranean sapropels (e.g., Slomp et al., 2004) and organic-rich sediments from the early Aptian OAE (Stein et al., 2011; Westermann et al., 2013) as well as Cenomanian/Turonian OAE (Mort et al., 2007; Kraal et al.,

2010), which received a sudden increase of OM. However, as discussed above, a part of the total P contents in sediments deposited under anoxic conditions might also be driven by the abundance of phosphatic fish debris (Schenau and De Lange, 2001), which may either accumulate in sediments due to combination of several environmental factors such as high production of fish debris in productive surface waters, abrupt fish mortality and efficient preservation under anoxic conditions. Indeed, according to selective extraction data from eastern Mediterranean (Slomp et al., 2004) and Arabian Sea sediments (Schenau and de Lange, 2000, 2001) anoxic bottom waters increase the preservation of phosphatic fish hard parts, becoming an important reactive P sink within the sediments (Slomp and Van Cappellen, 2007; Paytan and McLaughlin, 2007; März et al., 2014). In the Rietheim Posidonia Shale succession, thin sections analysis of black shale samples show the presence of phosphatic fish debris (Kuhn and Etter 1994). This would explain the good correlation between P_{total} and CFA contents through the entire section (Fig. 8d and Fig. 11g-h). Overall, our results suggest that changes in TOC/P_{total} molar ratios cannot be entirely attributed to changes in redox conditions in the Rietheim Posidonia Shale succession.

Alternatively, high P contents in organic-rich sediments deposited under anoxic conditions may also be related to the development of benthic microbial mats, such as coccoid bacteria and cryptalgal (Tribovillard et al., 2010; Westermann et al., 2013). In fact, the presence of abundant biomass in the sediment together with the development of microbial mats at the sediment–water interface might have limited the exchanges between the water column and the pore space within sediment, hampering pore water renewal and promoting the quantitative trapping of remobilized P in the sediment during redox recycling. This environmental process has been recently proposed to operate during the deposition of Jurassic organic-rich carbonates from the French Jura Mountains (Tribovillard et al., 2010).

6. Conclusions

The results of this high-resolution geochemical-mineralogical research allow for the following generalizations and conclusions:

1. Carbon isotope ($\delta^{13}C_{org\text{-}corr}$, $\delta^{13}C_{CaCO3}$), Rock-Eval pyrolysis, and TOC_{cff} data provide clear evidence that the pronounced ~3‰ negative CIE recorded in the Rietheim Posidonia Shale succession during the onset of the T-OAE mainly reflects a major perturbation in the global carbon cycle, likely induced by a massive injection of ^{13}C-depleted carbon into the whole exchangeable carbon reservoir, rather than changes in the type of OM and/or degree of stratification of bottom waters.
2. The Rock-Eval pyrolysis data and $\delta^{13}C_{org}$-$\delta^{15}N_{total}$ crossplots suggest that the OM in the upper Pliensbachian and lower Toarcian interval is primarily of terrestrial and marine origin, respectively, and deposited in an epicontinental sea setting.
3. The detrital proxies [notably, detritus index, siliciclastic balance and $Ln(Al_2O_3/Na_2O)$] corroborate that the elevated pCO_2 levels and greenhouse climate prevailing during the T-OAE induced an acceleration of the hydrologic cycle and an increase in chemical weathering rates.
4. The redox-sensitive proxies [notably, relative pyrite contents, organic and sulfide balances, V/(V+Ni) ratios, RSTE enrichment factors, Al-normalized RSTE versus TOC co-variation patterns, and TOC/P_{total} molar ratios] suggest that the sedimentary deposition of the Rietheim Posidonia Shale succession took place under oxic-to-dysoxic bottom-water conditions, slightly shifting toward anoxic and possibly euxinic conditions during the negative CIE. The T-OAE influence on the sedimentary environment prevailed until at least to the *bifrons* Zone. Overall, our results further support the idea that the influx of brackish Arctic seawater through the Viking Corridor could have facilitated the thermohaline stratification and subsequent dysoxic-to-anoxic bottom-water conditions within the NW Tethys Ocean (Dera and Donnadieu, 2012).

5. Enhanced rainfall and river freshwater inputs together with recurrent discharges of boreal brackish seawaters into the NW Tethys through the Viking Corridor (Dera and Donnadieu, 2012), appear to be a plausible scenario for explaining the P-enrichments (mainly authigenic P) in the Rietheim Posidonia Shale sediments during the early Toarcian warming event.
6. The geochemical characteristics of organic-rich sediments from the *exaratum* subzone suggest they were likely deposited in a sedimentary environment very similar to the Black Sea and/or Mediterranean sapropels.

Taken as a whole, our high-resolution geochemical and mineralogical data provide a solid record of the major palaeoenvironmental changes that fostered deposition of the Rietheim Posidonia Shale succession within the NW Tethys Ocean during the development of the T-OAE, and corroborate that deposition of the lower Toarcian black shales was mainly driven by a global climate change even though it was influenced by local environmental changes.

Acknowledgements

This research was funded through the GeoNova project and Université de Lausanne, with the financial support of the Swiss University Conference (CUS). We acknowledge Jean-Claude Lavanchy (Centre d'Analyse Minérale, UNIL), Hassan Saleh Khozyem/Tiffany Monnier (ISTE-UNIL) and Brahimsamba Bomou (ISTE-UNIL) for their support with the XRF, Rock-Eval and elemental analyses, respectively. We thank Thomas Algeo (University of Cincinnati) for his comments and suggestions, which significantly helped to improve the early version of this work. We further thank Christine Laurin for reviewing the grammar. Lastly, we specially thank the editor Finn Surlyk and the reviewer Matías Reolid (Universidad de Jaén) for their constructive and helpful comments, which significantly improved this work.

Appendix A. Supplementary material

Supplementary data associated with this article can be found in the online version at http…

File Excel. Rietheim Posidonia Shale dataset.exe

References

Anderson, L.D., Delaney, M.L., 2001. Carbon to phosphorus ratios in sediments: implications for nutrient cycling. Global Biogeochemical Cycles 15, 65-79.

Aitchison, J., 1986. The statistical analysis of compositional data. Monographs on statistics and applied probability. Chapman & Hall Ltd., London; reprinted in 2003 by the Blackburn Press, New Jersey, 416 p.

Algeo, T.J., Wilkinson, B.H., Lohmann, K.C, 1992. Meteoric-burial diagenesis of Pennsylvanian carbonate: water/rock interactions and basin geothermics. Journal of Sedimentary Petrology 62, 652-670.

Algeo, T.J., Maynard, J.B., 2004. Trace-element behavior and redox facies in core shales of Upper Pennsylvanian Kansas-type cyclothems. Chemical Geology 206, 289-318.

Algeo, T.J., Ingall, E., 2007. Sedimentary Corg:P ratios, paleocean ventilation, and Phanerozoic atmospheric pO2. Palaeogeography, Palaeoclimatology, Palaeoecology, 256, 130-155.

Algeo, T.J., Tribovillard, N., 2009. Environmental analysis of paleoceanographic systems based on molybdenum–uranium covariation. Chemical Geology 268, 211-225.

Algeo, T. J., Meyers, P. A., Robinson, R. S., Rowe, H., and Jiang, G. Q., 2014. Icehouse–greenhouse variations in marine denitrification. Biogeosciences 11, 1273-1295.

Al-Suwaidi, A.H., Angelozzi, G.N., Baudin, F., Damborenea, S.E., Hesselbo, S.P., Jenkyns, H.C., Manceñido, M.O., Riccardi, A.C., 2010. First record of the Early Toarcian Oceanic Anoxic Event

from the Southern Hemisphere, Neuquén Basin, Argentina. Journal of the Geological Society of London 167, 633-636.

Arthur, M.A., Jenkyns, H.C., Brumsack, H.-J., Schlanger, S.O., 1990. Stratigraphy, geochemistry, and paleoceanography of organic-carbon rich Cretaceous sequences. In: Ginsburg, R.N., Beaudoin, B. (Eds.), Cretaceous Research. Events and Rhythms Kluwer Acad, Norwell, pp. 75-119.

Baudin, F., Herbin, J.-P., Vandenbroucke, M., 1990a. Mapping and geochemical characterization of Toarcian organic matter in the Mediterranean Tethys. Organic Geochemistry 16, 677-687.

Baudin, F., Herbin, J.-P., Bassoullet, J.-P., Dercourt, J., Lachkar, G., Manivit, H. and Renard, M. 1990b. Distribution of organic matter during the Toarcian in the Mediterranean Tethys and Middle East. 73–92. In HUC, A. Y. (ed.). Deposition of organic facies. Vol. 30. American Association of Petroleum Geologists, Tulsa, 234 pp.

Beerling, D. J., Brentnall, S. J., 2007. Numerical evaluation of mechanisms driving Early Jurassic changes in global carbon cycling. Geology 35, 247-250.

Benitez-Nelson, C.R., 2000. The biogeochemical cycling of phosphorus in marine systems. Earth-Science Reviews 51, 109-135.

Bernoulli, D., Jenkyns, H.C., 2009. Ancient oceans and continental margins of the Alpine–Mediterranean Tethys: deciphering clues from Mesozoic pelagic sediments and ophiolites. Sedimentology 56, 149-190.

Behar, F., Beaumont, V., Penteado, H.L.D., 2001. Rock-Eval 6 technology: performances and developments. Oil and Gas Science and Technology 56, 111-134.

Bodin, S., Godet, A., Matera, V., Steinmann, P., Vermeulen, J., Gardin, S., Adatte, T., Coccioni, R., Föllmi, K.B., 2006. Enrichment of redox-sensitive trace metals (U, V, Mo, As) associated with the late Hauterivian Faraoni oceanic anoxic event. International Journal of Earth Sciences (Geologische Rundschau) 96, 327-341.

Bodin, S., Mattioli, E., Fröhlich, S., Marshall, J.D., Boutib, L., Lahsini, S., Redfern, J., 2010. Toarcian carbon isotope shifts and nutrient changes from the Northern margin of Gondwana (High Atlas, Morocco, Jurassic): palaeoenvironmental implications. Palaeogeography, Palaeoclimatology, Palaeoecology 297, 377-390.

Bomou, B., Adatte, T., Tantawy, A. A., Mort, H., Fleitmann, D., Huang, Y., Föllmi, K.B., 2013. The expression of the Cenomanian–Turonian oceanic anoxic event in Tibet. Palaeogeography, Palaeoclimatology, Palaeoecology 369, 466-481.

Brumsack, H.-J., 1991. Inorganic geochemistry of the German Posidonia Shale: paleoenvironmental consequences. In: Modern and Ancient Continental Shelf Anoxia (R.V. Tyson & T.H. Pearson, Edts.), Geological Society, London, Special Publications 58, 353-362.

Calvert, S.E., Pedersen, T.F., 2007. Elemental proxies for palaeoclimatic and palaeoceanographic variability in marine sediments: interpretation and application. In: Hillaire-Marcel, C., Vernal, A.D. (Eds.), Proxies in Late Cenozoic Paleoceanography. Elsevier, Amsterdam, pp. 567–644.

Caruthers, A.H., Gröcke, D.R., Smith, P.L., 2011. The significance of an early Jurassic (Toarcian) carbon isotope excursion in Haida Gwaii (Queen Charlotte Islands), British Columbia, Canada. Earth and Planetary Science Letters 307, 19-26.

Chandler, M.A., Rind, D., Ruedy, R., 1992. Pangaean climate during the Early Jurassic: GCM simulations and the sedimentary record of paleoclimate. Geological Society of America Bulletin 104, 543-559.

Cohen, A.S., Coe, A.L., Harding, S.M., Schwark, L., 2004. Osmium isotope evidence for the regulation of atmospheric CO2 by continental weathering. Geology 32, 157-160.

Cullers, R. L., 2000. The geochemistry of shales, siltstones and sandstones of Pennsylvian-Permian age, Colorado, USA: implications for provenance and metamorphic studies. Lithos 51, 181–203.

Dean, W.E., Arthur, M.A., Claypool, G.E., 1986. Depletion of 13C in Cretaceous marine organic matter: source, diagenetic, or environmental signal? Marine Geology 70, 119-157.

Delaney, M.L., 1998. Phosphorus accumulation in marine sediments and the oceanic phosphorus cycle. Global Biogeochemical Cycles 12, 563-572.

Dera, G., Pellenard, P., Neige, P., Deconinck, J.-F., Pucéat, E., Dommergues, J.-L., 2009. Distribution of clay minerals in Early Jurassic Peritethyan seas: palaeoclimatic significance inferred from multiproxy comparisons. Palaeogeography, Palaeoclimatology, Palaeoecology 271, 39-51.

Dera, G., Brigaud, B., Monna, F., Laffont, R., Pucéat, E., Deconinck, J.-F., Pellenard, P., Joachimski, M.M., Durlet, C., 2011. Climatic ups and downs in disturbed Jurassic world. Geology 39, 215-218.

Dera, G., Donnadieu, Y., 2012. Modeling evidences for global warming, Arctic seawater freshening, and sluggish oceanic circulation during the Early Toarcian anoxic event. Paleoceanography 27, PA2211, doi:10.1029/2012PA002283.

Duncan, R.A., Hooper, P.R., Rahacek, J., Marsh, J.S. & Duncan, A.R., 1997. The timing and duration of the Karoo igneous event, southern Gondwana. Journal of Geophysical Research, 102, 18127-18138.

Eberl, D.D., 2003. User guide to RockJock—a program for determining quantitative mineralogy from X-ray diffraction data. USGS Open File Report OF 03-78. 40 pp.

Egozcue, J.J., Pawlowsky-Glahn, V., 2005. Group of parts and their balances in compositional data analysis. Mathematical Geology 37, 795-828.

Föllmi, K.B., 1996. The phosphorus cycle, phosphogenesis and marine phosphate-rich deposits. Earth-Science Reviews 40, 55-124.

Goldberg, K., Humayun, M., 2010. The applicability of the chemical index of alteration as a paleoclimatic indicator: An example from the Permian of the Paraná Basin, Brazil. Palaeogeography, Palaeoclimatology, Palaeoecology 293, 175–183.

Gröcke, D.R., Hori, R. S., Trabucho-Alexandre, J., Kemp, D. B., Schwark, L., 2011. An open ocean record of the Toarcian oceanic anoxic event. Solid Earth 2, 245-257.

Hatch, J.R., Leventhal, J.S., 1992. Relationship between inferred redox potential of the depositional environment and geochemistry of the Upper Pennsylvanian (Missourian) Stark Shale Member of the Dennis Limestone, Wabaunsee County, Kansas, U.S.A. Chemical Geology 99, 65–82.

Hallam, A., 2001. A review of broad pattern of the Jurassic sea-level changes and their possible causes in the light of current knowledge. Palaeogeography, Palaeoclimatology, Palaeoecology167, 23-37

Hardenbol, J., Thierry, J., Farley, M.B., de Graciansky, P.-C., Vail, P.R., 1998. Mesozoic and Cenozoic sequence chronostratigraphic framework of European basins. In: de Graciansky, P.-C., Hardenbol, J., Jacquin, T., Vail, P.R. (Eds.), Mesozoic and Cenozoic Sequence Stratigraphy of European basins. Special Publication, Society for Sedimentary Geology, vol. 60, pp. 3-13.

Hermoso, M., Le Callonnec, L., Minoletti, F., Renard, M., Hesselbo, S.P., 2009a. Expression of the Early Toarcian negative carbon-isotope excursion in separated carbonate microfractions (Jurassic, Paris Basin). Earth and Planetary Science Letters 277, 194-203.

Hermoso, M., Minoletti, F., Le Callonnec, L., Jenkyns, H.C., Hesselbo, S.P., Rickaby, R.E.M., Renard, M., de Rafélis, M., Emmanuel, L., 2009b. Global and local forcing of Early Toarcian seawater chemistry: a comparative study of different paleoceanographic settings (Paris and Lusitanian basins). Paleoceanography 24, PA4208, doi:10.1029/2009PA001764.

Hermoso, M., Minoletti, F., Pellenard, P., 2013. Black shale deposition during Toarcian super-greenhouse driven by sea level. Climate of the Past 9, 2703-2712.

Hermoso, M., Pellenard, P., 2014. Continental weathering and climatic changes inferred from clay mineralogy and paired carbon isotopes across the early to middle Toarcian in the Paris Basin. Palaeogeography, Palaeoclimatology, Palaeoecology 399, 385–393.

Hesselbo, S.P., Jenkyns, H.C., 1998. British Lower Jurassic sequence stratigraphy. In: DeGraciansky, P.-C., Hardenbol, J., Jacquin, T., Vail, P.R., Farley, M.B. (Eds.), Sequence Stratigraphy of European Basins: Special Publication of the SEPM, 60, pp. 561-581.

Hesselbo, S.P., Gröcke, D.R., Jenkyns, H.C., Bjerrum, C.J., Farrimond, P., Morgans Bell, H.S., Green, O.R., 2000. Massive dissociation of gas hydrate during a Jurassic oceanic anoxic event. Nature 406, 392-395.

Hesselbo, S.P., Jenkyns, H.C., Duarte, L.V., Oliveira, L.C.V., 2007. Carbon-isotope record of the Early Jurassic (Toarcian) Oceanic Anoxic Event from fossil wood and marine carbonate (Lusitanian Basin, Portugal). Earth and Planetary Science Letters 253, 455-470.

Hoffman, D.L., Algeo, T.J., Maynard, J.B., Joachimski, M.M., Hower, J.C., and Jaminski, J., 1998. Regional and stratigraphic variation in bottomwater anoxia in offshore core shales of Upper Pennsylvanian cyclothems from the Eastern Midcontinent Shelf (Kansas), USA. In: Schieber, J., Zimmerle, W., and Sethi, P.S., eds., Shales and Mudstones, v. 1: Stuttgart, Schweizerbart'sche, p. 243-269.

Immenhauser, A., Schreurs, G., Peters, T., Matter, A., Hauser, M., Dumitrica, P., 1998. Stratigraphy, sedimentology, and depositional environments of the Permian to uppermost Cretaceous Batain Group, eastern Oman. Eclogae geologicae Helvetiae 91, 217–235.

Ingall, E., Kolowith, L., Lyons, T., Hurtgen, M., 2005. Sediment carbon, nitrogen and phosphorus cycling in an anoxic fjord, Effingham Inlet, British Columbia. American Journal of Science 305, 240-258.

Irino, T., Pedersen, T. 2000. Geochemical character of glacial to interglacial sediments at Site 1017, southern Californian Margin: Minor and trace elements. Proc. Ocean Drill. Program Sci. Results 167, 263-271.

Izumi , K., Miyaji, T., Tanabe, K., 2012. Early Toarcian (Early Jurassic) oceanic anoxic event recorded in the shelf deposits in the northwestern Panthalassa: evidence from the Nishinakayama Formation in the Toyora area, west Japan. Palaeogeography, Palaeoclimatology, Palaeoecology 315-316, 100-108.

Jaminski, J., Algeo, T.J., Maynard, J.B., and Hower, J.C., 1998. Climatic origin of dm-scale compositional cyclicity in the Cleveland Member of the Ohio Shale (Upper Devonian), Central Appalachian Basin, USA. In: Schieber, J., Zimmerle, W., and Sethi, P.S., eds., Shales and Mudstones, v. 1: Stuttgart, Schweizerbart'sche, p. 217-242.

Jenkyns, H.C., 1988. The early Toarcian (Jurassic) event: stratigraphy, sedimentary, and geochemical evidence. American Journal of Science 288, 101-151.

Jenkyns, H.C., Gröcke, D., Hesselbo, S.P., 2001. Nitrogen isotope evidence for water mass denitrification during the early Toarcian Oceanic Anoxic Event. Paleoceanography, 16, 593-603.

Jenkyns, H.C., Jones, C.E., Gröcke, D.R., Hesselbo, S.P., Parkinson, D.N., 2002. Chemostratigraphy of the Jurassic system: applications, limitations and implication for palaeoceanography. Journal of the Geological Society 159, 351-378.

Jenkyns, H.C., 2010. Geochemistry of oceanic anoxic events. Geochemistry, Geophysics, Geosystems 11, Q03004, doi:10.1029/2009GC002788.

Jones, B., Manning, D.A.C., 1994. Comparison of geochemical indices used for the interpretation of palaeoredox conditions in ancient mudstones. Chemical Geology 111, 111–129.

Keller, G., Pardo, A., 2004. Age and paleoenvironment of the Cenomanian–Turonian global stratotype section and point at Pueblo, Colorado. Marine Micropaleontology 51, 95-128.

Kemp, D.B., Coe, A.L., Cohen, A.S., Schwark, L., 2005. Astronomical pacing of methane release in the Early Jurassic period. Nature 437, 396-399.

Kraal, P., Slomp, C.P., Forster, A., Kuypers, M.M.M., 2010. Phosphorus cycling from the margin to abyssal depths in the proto-Atlantic during oceanic anoxic event 2. Palaeogeography, Palaeoclimatology, Palaeoecology 295, 42-54.

Kuhn, O., Etter, W., 1994. Der Posidonienschiefer der Nordschweiz: Lithostratigraphie, Biostratigraphie und Fazies. Eclogae Geologicae Helvetiae 87, 113-138.

Küspert, W., 1982. Environmental change during oil shale deposition as deduced from stable isotope ratios. In: Einsele, S., Seilacher, A. (Eds.), Cyclic and event stratification. Springer, New York, pp. 482-501.

März C., Poulton, S.W., Wagner, T., Schnetger, B., Brumsack, H-J., 2014. Phosphorus burial and diagenesis in the central Bering Sea (Bowers Ridge, IODP Site U1341): Perspectives on the marine P cycle. Chemical Geology 363, 270-282.

Mattioli, E., Pittet, B., Suan, G., Mailliot, S., 2008. Calcareous nannoplankton across the Early Toarcian Anoxic Event: implications for paleoceanography within the western tethys. Paleoceanography 23, PA3208, DOI: 10.1029/2007PA001435.

Mattioli, E., Pittet, B., Petitpierre, L., Mailliot, S., 2009. Dramatic decrease of pelagic carbonate production by nannoplankton across the Early Toarcian anoxic event (T-OAE). Global and Planetary Change 65, 134-145.

McArthur, J.M., Algeo, T.J., van de Schootbrugge, B., Li, Q., Howarth, R.J., 2008. Basinal restriction, black shales, Re–Os dating, and the Early Toarcian (Jurassic) oceanic anoxic event. Paleoceanography 23, PA4217.

McElwain, J.C.,Wade-Murphy, J., Hesselbo, S.P., 2005. Changes in carbon dioxide during an oceanic anoxic event linked to intrusion into Gondwana coals. Nature 435, 479-482.

Montero-Serrano, J.C., Palarea-Albaladejo, J., Martín-Fernández, J.A., Martínez-Santana, M., Gutiérrez-Martín, J.V., 2010. Sedimentary chemofacies characterization by means of multivariate analysis. Sedimentary Geology 228, 218-228.

Mort, H., Adatte, T., Föllmi, K., Keller,, Steinmann, P., Matera V., Berner, Z., And Stüben, D., 2007. Phosphorus and the roles of productivity and nutrient recycling during Oceanic Anoxic Event 2. Geology 35-6, 483-486.

Murray, J. W., Jannasch, H. W., Honjo, S., Anderson, R. F., Reeavrcn, W. S., Top, Z., Friederich, G. E., Codispoti, L. A., Izdar, E., 1989. Unexpected changes in the oxic/anoxic interface in the Black Sea. Nature 338, 411-413.

Nesbitt, H.W., Young, G.M., 1982. Early Proterozoic climates and plate motions inferred from major element chemistry of lutites. Nature 299, 715–717.

Pálfy, J., Smith, P.L., 2000. Synchrony between Early Jurassic extinction, oceanic anoxic event, and the Karoo-Ferrar flood basalt volcanism. Geology 28, 747-750.

Parrish, J.T., Curtis, R.L., 1982. Atmospheric circulation, upwelling, and organic-rich rocks in the Mesozoic and Cenozoic areas. Palaeogeography, Palaeoclimatology, Palaeoecology 40, 31-66.

Paytan, A. and McLaughlin, K., 2007. The oceanic phosphorus cycle. Chemical Review 107, 563–576.

Pawlowsky-Glahn, V., Egozcue, J., 2011. Exploring compositional data with the CoDa-dendrogram. Austrian Journal of Statistics 40, 103-113.

Pearce, C.R., Cohen, A.S., Coe, A.L., Burton, K.W., 2008. Molybdenum isotope evidence for global ocean anoxia coupled with perturbations to the carbon cycle during the Early Jurassic. Geology 36, 231-234.

Piper, D.Z., Dean, W.E., 2002. Trace-element deposition in the Cariaco Basin under sulfate reducing conditions - a history of the local hydrography and global climate, 20 ka to the present. US Geological Survey Professional Paper 1670, 41pp.

Perilli, N., 2000. Calibration of early–middle Toarcian nannofossil events based on high resolution ammonite biostratigraphy in two expanded sections from the Iberian Range (East Spain). Marine Micropaleontology 39, 293–308.

Pittet, B., Suan, G., Lenoir, F., Duarte, L.V., Mattioli, E., 2014. Carbon isotope evidence for sedimentary discontinuities in the lower Toarcian of the Lusitanian Basin (Portugal): Sea level change at the onset of the Oceanic Anoxic Event. Sedimentary Geology 303, 1–14.

Prauss, M., Ligouis, B., Luterbacher, H., 1991. Organic matter and palynomorphs in the 'Posidonienschiefer' (Toarcian, Lower Jurassic) of southern Germany. Journal Geological Society London Special Publications 58, 335-351.

Reátegui, K., Martínez, M., Esteves, I., Gutiérrez, J.V., Martínez, A., Meléndez, W., Urbani, F., 2005. Geochemistry of the Mirador Formation (Late Eocene-Early Oligocene), south western Venezuela: chemostratigraphic constraints on provenance and the influence of the sea level. Geochemical Journal 39 (3), 213-226.

Redfield, A.C., 1958. The biological control of chemical factors in the environment. American Scientist 46, 205-222.

Reimann, C., Filzmoser, P., Garrett, R.G., Dutter, R., 2008. Statistical Data Analysis Explained - Applied environmental statistics with R. John Wiley, Chichester, 362 pp.

Reisdorf, A. G., Wetzel, A., Schlatter, R., & Jordan, P., 2011. The Staffelegg Formation: a new stratigraphic scheme for the Early Jurassic of northern Switzerland. Swiss Journal of Geosciences 104 , 97-146.

Reolid, M., Rodríguez-Tovar, F.J., Marok, A., Sebane, A., 2012. The Toarcian Oceanic Anoxic Event in the Western Saharan Atlas, Algeria (North African Paleomargin): role of anoxia and productivity. Geological Society of America Bulletin 124, 1646-1664.

Reolid, M., Marok, A., Sebane, A., 2014a. Foraminiferal assemblages and geochemistry for interpreting the incidence of Early Toarcian environmental changes in North Gondwana palaeomargin (Traras Mountains, Algeria). Journal of African Earth Sciences 95, 105-122.

Reolid, M., Mattioli, E., Nieto, L.M., Rodríguez-Tovar, F.J., 2014b. The Early Toarcian Ocanic Anoxic Event in the External Subbetic (Southiberian Palaeomargin, Westernmost Tethys): geochemistry, nannofossils and ichnology. Palaeogeography, Palaeoclimatology, Palaeoecology 411, 79-94.

Reolid, M., 2014. Stable isotopes on foraminifera and ostracods for interpreting incidence of the Toarcian Oceanic Anoxic Event in Westernmost Tethys: role of water stagnation and productivity. Palaeogeography, Palaeoclimatology, Palaeoecology 395, 77-91.

Rodríguez-Tovar, F.J., Reolid, M., 2013. Environmental conditions during the Toarcian Oceanic Anoxic Event (T-OAE) in the westernmost Tethys: influence of the regional context on a global phenomenon. Bulletin of Geosciences 88-4, 697–712.

Röhl, H.J., Schmid-Röhl, A., Oschmann, W., Frimmel, A., Schwark, L., 2001. The Posidonia Shale (Lower Toarcian) of SW-Germany: an oxygen-depleted ecosystem controlled by sea level and palaeoclimate. Palaeogeography, Palaeoclimatology, Palaeoecology 165, 27-52.

Röhl, H.-J., Schmid-Röhl, A., 2005. Lower Toarcian (Upper Liassic) black shales of the Central European Epicontinental Basin: a sequence stratigraphic case study from the SW German Posidonia Shale (Lower Toarcian). SEPM. Special Publication 82, 165-189.

Rosales, I., Quesada, S., Robles, S., 2004. Paleotemperature variations of Early Jurassic seawater recorded in geochemical trends of belemnites from the Basque–Cantabrian basin, northern Spain. Palaeogeography, Palaeoclimatology, Palaeoecology 203, 253–275.

Ruebsam, W., Münzbergerb, P., Schwarka, L., 2014. Chronology of the Early Toarcian environmental crisis in the Lorraine Sub-Basin (NE Paris Basin). Earth and Planetary Science Letters 404, 273–282.

Schenau, S.J. and de Lange, G.J., 2000. A novel chemical method to quantify fish debris in marine sediments. Limnology and Oceanography 45, 963-971.

Schenau, S.J. and de Lange, G.J., 2001. Phosphorus regeneration vs. burial in sediments of the Arabian Sea. Marine Chemistry 75, 201–207.

Schrag, D.P., DePaolo, D.J., Richter, F.M., 1995. Reconstructing past sea surface temperatures from oxygen isotope measurements of bulk carbonate. Geochimica et Cosmochimica Acta 59, 2265-2278.

Slomp, C.P., Thomson, J., De Lange, G., 2004. Controls on phosphorus regeneration and burial during formation of eastern Mediterranean sapropels. Marine Geology 203,141–159.

Slomp, C.P. and Van Cappellen, P., 2007. The global marine phosphorus cycle: sensitivity to oceanic circulation. Biogeosciences 4, 155-171.

Stein, M., Föllmi, K.B., Westermann, S., Godet, A., Adatte, T., Matera, V., Fleitmann, D., Berner, Z., 2011. Progressive palaeoenvironmental change during the Late BarremianeEarly Aptian as prelude to Oceanic Anoxic Event 1a: evidence from the Gorgo a Cerbara section (Umbria-Marche Basin, central Italy). Palaeogeography, Palaeoclimatology, Palaeoecology 302, 396-406.

Suan, G., Pittet, B., Bour, I., Mattioli, E., Duarte, L.V., Mailliot, S., 2008. Duration of the Early Toarcian carbon isotope excursion deduced from spectral analysis: consequence for its possible causes. Earth and Planetary Science Letters 267, 666-679.

Suan, G., Mattioli, E., Pittet, B., Lécuyer, C., Suchéras-Marx, B., Duarte, L.V., Philippe, M., Reggiani, M.L., Martineau, F., 2010. Secular environmental precursors to Early Toarcian (Jurassic) extreme climate changes. Earth and Planetary Science Letters 290, 448-458.

Suan, G., Nikitenko, B. L., Rogov, M. A., Baudin, F., Spangenberg, J. E., Knyazev, V. G., Glinskikh, L. A., Goryacheva, A. A., Adatte, T., Riding, B. J., Föllmi, K. B., Pittet, B., Mattioli, E., Lecuyer, C., 2011. Polar record of Early Jurassic massive carbon injection. Earth and Planetary Science Letters 312, 102-113.

Svensen, H., Planke, S., Chevallier, L., Malthe-Sørenssen, A., Corfu, F., Jamtveit, B., 2007. Hydrothermal venting of greenhouse gases triggering Early Jurassic global warming. Earth Planet. Sci. Lett. 256, 554–566.

Tada, R., Sato, S., Irino, T., Matsui, H., Kennett, J.P., 2000. Millennial-scale compositional variations in late Quaternary sediments at Site 1017, southern California. Proceedings of the Ocean Drilling Program - Scientific Results 167, 277-296.

Trecalli, A., Spangenberg, J.E., Adatte, T., Föllmi, K.B., Parente, M., 2012. Carbonate platform evidence of ocean acidification at the onset of the early Toarcian oceanic anoxic event. Earth and Planetary Science Letters 357-358, 214-225.

Tribovillard, N., Recourt, P., Trentesaux, A., 2010. Bacterial calcification as a possible trigger for francolite precipitation under sulfidic conditions. Comptes Rendus Geoscience 342-1, 27–35.

Tribovillard, N., Algeo, T.J., Lyons, T.W., Riboulleau, A., 2006. Trace metals as paleoredox and paleoproductivity proxies: an update. Chemical Geology 232, 12-32.

Van Cappellen, P., Ingall, E.D., 1994. Benthic phosphorus regeneration, net primary production, and ocean anoxia: a model of the coupled marine biogeochemical cycles of carbon and phosphorus. Paleoceanograpghy 9, 677-692.

van de Schootbrugge, B., McArthur, J.M., Bailey, T.R., Rosenthal, Y., Wright, J.D., Miller, K.G., 2005. Toarcian oceanic anoxic event: an assessment of global causes using belemnite C isotope records. Paleoceanography 20, PA3008. doi:10.1029/2004PA001102.

van de Schootbrugge, B., Bachan, A., Suan, G., Richoz, S., Payne, J. L., 2013. Microbes, mud and methane: cause and consequence of recurrent Early Jurassic anoxia following the end-Triassic mass extinction. Palaeontology 56, 685–709.

van den Boogaart, K.G., Tolosana-Delgado, R., 2008. “Compositions”: a unified R package to analyze compositional data. Computers and Geosciences 34, 320-338.

von Eynatten, H., Barcelo-Vidal, C., Pawlowsky-Glahn, V., 2003. Modelling compositional change: the example of chemical weathering of granitoid rocks. Mathematical Geology 35, 231–251.

Vrielynck, B., Bouysse, P., 2003. The Changing Face of the Earth. Commission for the Geological Map of the World, CCGM-UNESCO Publishing. 32 p., 11 pl.

Warning, B., Brumsack, H.J., 2000. Trace metal signatures of eastern Mediterranean sapropels. Palaeogeography, Palaeoclimatology, Palaeoecology 158, 293-309.

Wedepohl, K.H., 1991. The composition of the upper Earth's crust and the natural cycles of selected elements. Metals in natural raw materials. Natural resources. In: Merian, E. (Ed.), Metals and their Compounds in the Natural Environment. VCH, Weinheim, Germany, pp. 3-17.

Westermann, S., Caron, M., Fiet, N., Fleitmann, D., Matera, V., Adatte, T., Föllmi, K.B., 2010. Evidence for oxic conditions during oceanic anoxic event 2 in the northern Tethyan pelagic realm. Cretaceous Research 31, 500-514.

Westermann S., Stein M., Matera V., Fiet N., Fleitmann D., Adatte T., Föllmi K.B., 2013. Rapid changes in the redox conditions of the western Tethys Ocean during the OAE 1a interval (early Aptian). Geochimica et Cosmochimica Acta 121, 467-486.

Wignall, P.B., Newton, R.J., Little, C.T.S., 2005. The timing of paleoenvironmental change and cause-and-effect relationships during the Early Jurassic mass extinction in Europe. American Journal of Science 305, 1014-1032

Wignall, P.B., McArthur, J.M., Little, C.T.S., Hallam, A., 2006. Palaeoceanography: methane release in the Early Jurassic period. Nature 441, E5, doi:10.1038/nature04905.

Figure captions

Figure 1. (**a**) Palaeogeographical maps for the early Toarcian (redrawn from Vrielynck and Bouysse, 2003) showing the main large igneous provinces (Karoo-Ferrar and North Sea), the Viking Corridor, the NW Tethyan region, and the Rietheim Posidonia Shale succession studied herein. VC indicates the location of the Viking Corridor. Locations of the Lower Toarcian successions discussed in this study are noted as black circles: Dotternhausen, SW Germany (D; Röhl et al., 2001); Schesslitz, SW Germany (S; Küspert, 1982; Prauss et al., 1991); Yorkshire, England (Y; Cohen et al., 2004; Kemp et al., 2005); and Kelimyar River, N Siberia (KR; Suan et al., 2011). (**b**) Map showing the location of the Rietheim Posidonia Shale succession and geological setting in northern Switzerland.

Figure 2. Biostratigraphy and lithostratigraphy for the upper Pliensbachian to lower Toarcian interval at the Rietheim Posidonia Shale succession. The ammonite biostratigraphy is from Kuhn and Etter (1994). Photographs of the drill core and its stratigraphic position are also shown.

Figure 3. Stratigraphic distribution of the: isotopic compositions of (**a-b**) carbon ($\delta^{13}C_{org}$, $\delta^{13}C_{CaCO3}$), (**c**) oxygen ($\delta^{18}O_{CaCO3}$), (**d**) nitrogen ($\delta^{15}N_{total}$), (**e**) total organic carbon (TOC), (**f**) total organic carbon from the carbonate-free fraction (TOC_{cff}), (**g**) hydrogen index (HI), and (**h**) Rock-Eval T_{max} from the Rietheim Posidonia Shale succession. The shaded interval indicates the negative carbon isotope excursion (CIE) related to the T-OAE.

Figure 4. (**a**) Hydrogen Index (HI) vs. Oxygen Index (OI) crossplot illustrating the organic matter origin of the Rietheim Posidonia Shale samples. Note that the organic matter was primarily of marine origin during the lower Toarcian (e*xaratum* to *commune* subzones). (**b**) $\delta^{13}C_{org}$-HI crossplots. The least square

linear regression is based on samples from outside of the T-OAE. Note that $\delta^{13}C_{org}$ values slightly decrease with increasing HI values. (**c**) $\delta^{13}C_{org}$-$\delta^{15}N_{total}$ crossplots showing the depositional settings of the Rietheim Posidonia Shale sediments. The average $\delta^{13}C_{org}$-$\delta^{15}N_{total}$ values of the five depositional settings are from Algeo et al. (2014).

Figure 5. Comparison between the bulk $\delta^{13}C_{org}$ records **(a)** with $\delta^{13}C_{org}$ corrected for changing OM sourcing **(b)** and $\delta^{13}C_{CaCO3}$ **(c)**. Note that the bulk organic C-isotope data were corrected using the HI and raw C-isotope data from the *spinatum* and *bifrons* zones. The blue, red and black lines represent the 9-point moving average of the isotopic data.

Figure 6. X-ray diffractograms of typical bulk rock samples from the early Toarcian negative carbon isotope excursion (CIE) in the Rietheim Posidonia Shale succession.

Figure 7. Stratigraphic distribution of the bulk mineralogical semiquantification from the Rietheim Posidonia Shale sediments. The shaded interval indicates the negative carbon isotope excursion (CIE) related to the T-OAE.

Figure 8. (**a-d**) Stratigraphic profiles of the major geochemical associations obtained by the compositional Q-mode cluster analysis. The shaded interval indicates the negative carbon isotope excursion (CIE) related to the T-OAE. The red lines represent the 9-point moving average of the data. (**e**) Dendrogram of association of variables obtained by applying Ward clustering algorithm based on the variation matrix of elemental geochemical dataset.

Figure 9. Overview of upper Pliensbachian to lower Toarcian carbon-isotope records from representative Tethyan and Boreal successions. Carbon-isotope data from (**a**) Rietheim Posidonia Shale, N Switzerland (this study; the black line represent the 9-point moving average of the isotopic data), (**b**) Dotternhausen and Zimmern, SW Germany (modifed from Küspert, 1982; Prauss et al., 1991 and Röhl et al., 2001), (**c**) Yorkshire, England (Cohen et al., 2004; Kemp et al., 2005) and (**d**) Kelimyar River, N Siberia (Suan et al., 2011). See Fig. 1a for the geographical location of these stratigraphic sections. The shaded interval indicates the negative carbon isotope excursion (CIE) related to the T-OAE. Note that carbon-isotope profiles in geographically distant sections exhibit a similar trend in the lower Toarcian interval.

Figure 10. Stratigraphic distribution of the main detrital proxies obtained from the Rietheim Posidonia Shale succession. (**a**) detritus index (summing of quartz, phyllosilicates, K-feldspars, Na-plagioclases); (**b**) Ln(Al_2O_3/Na_2O); (**c**) XRF siliciclastic balance (Nb, Rb, La, K, Ti, Al, Si, Cr, Na, Y, Nd). Balances are represents according to equation 1 (see Section 3.2.5). The red lines represent the 9-point moving average of the data. The shaded interval indicates the negative carbon isotope excursion (CIE) related to the T-OAE.

Figure 11. Stratigraphic distribution of the main redox proxies obtained from the Rietheim Posidonia Shale succession. (**a**) relative content of pyrite (%); (**b-c**) sulphide (Zn, Cu, Fe, Co) and OM (P, As, TOC, Ni, V) balances. Balances are represents according to equation 1 (see Section 3.2.5); (**d**) V/(V+Ni) ratios. Redox zones are from Hatch and Leventhal (1992); (**e-f**) elements enrichment factors (EF) for the OM and sulphide associations; (**g**) relative content of fluorapatite (%); (**h**) TOC and total phosphorus (P_{total}) relationship (TOC/P_{total}). The red lines represent the 9-point moving average of the data. The shaded interval indicates the negative carbon isotope excursion (CIE) related to the T-OAE.

Figure 12. Al-normalized redox-sensitive trace-elements (V, Ni, As and Cu) plotted versus total organic carbon from the Rietheim Posidonia Shale sediments. This plot is used to discriminate between different redox facies (dysoxic, anoxic and euxinic; e.g., Algeo and Maynard, 2004; Trivovillard et al., 2006). Redox-sensitive trace-metal data from the Cariaco Basin (Piper and Dean, 2002), the Southern California margin (Irino and Pedersen, 2000; Tada et al., 2000), Posidonia Shale from SW Germany (Brumsack, 1991), upper Pennsylvanian black shales (Algeo and Maynard, 2004), and Mediterranean and Black Sea sapropels (Warning and Brumsack, 2000) are also plotted.

Highlights

-The T-OAE negative CIE reflects a ^{13}C-depleted carbon injection to ocean-atmosphere

-Detrital proxies suggest an increase in continental weathering rates during the T-OAE

-Redox proxies suggest moderate anoxic bottom-water conditions during the T-OAE

-Dysoxic-to-anoxic conditions prevailed until at least to the *bifrons* Zone

-P-enrichments are observed during the T-OAE

Figure 1

Figure 1

(Double column - full page width)

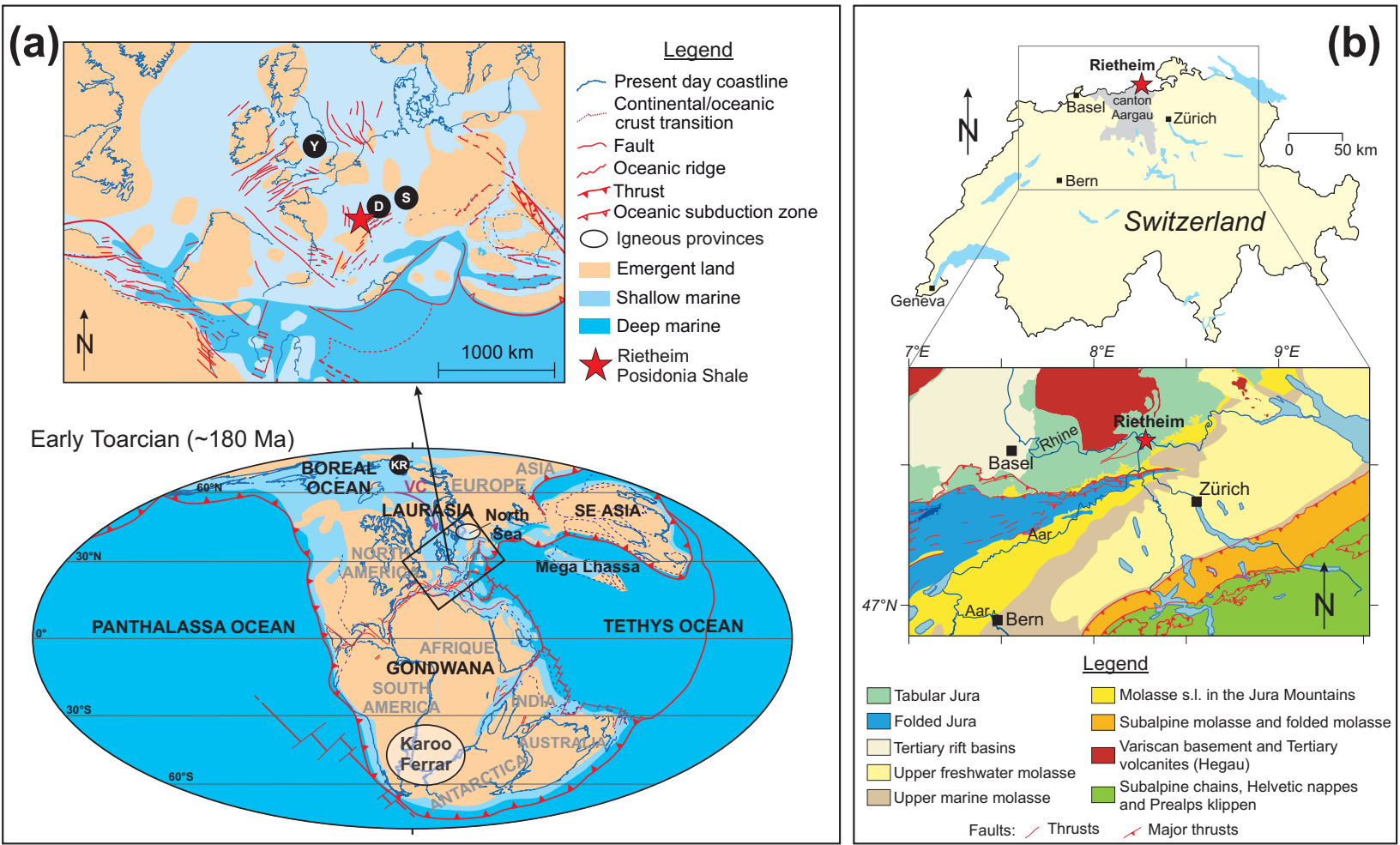

Figure 2

Figure 2

(1.5 column)

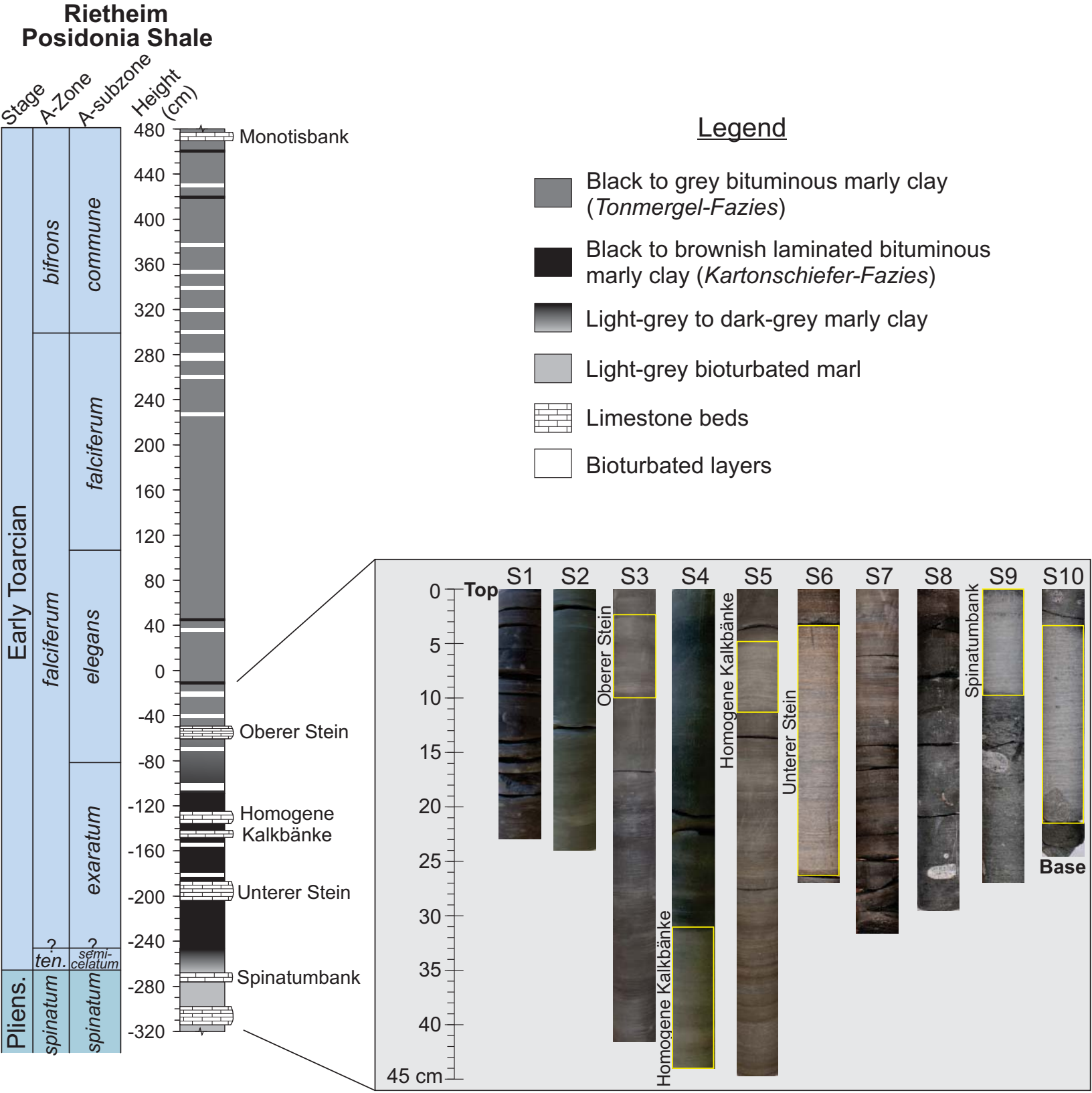

Figure 3

Figure 3

(Double column - full page width)

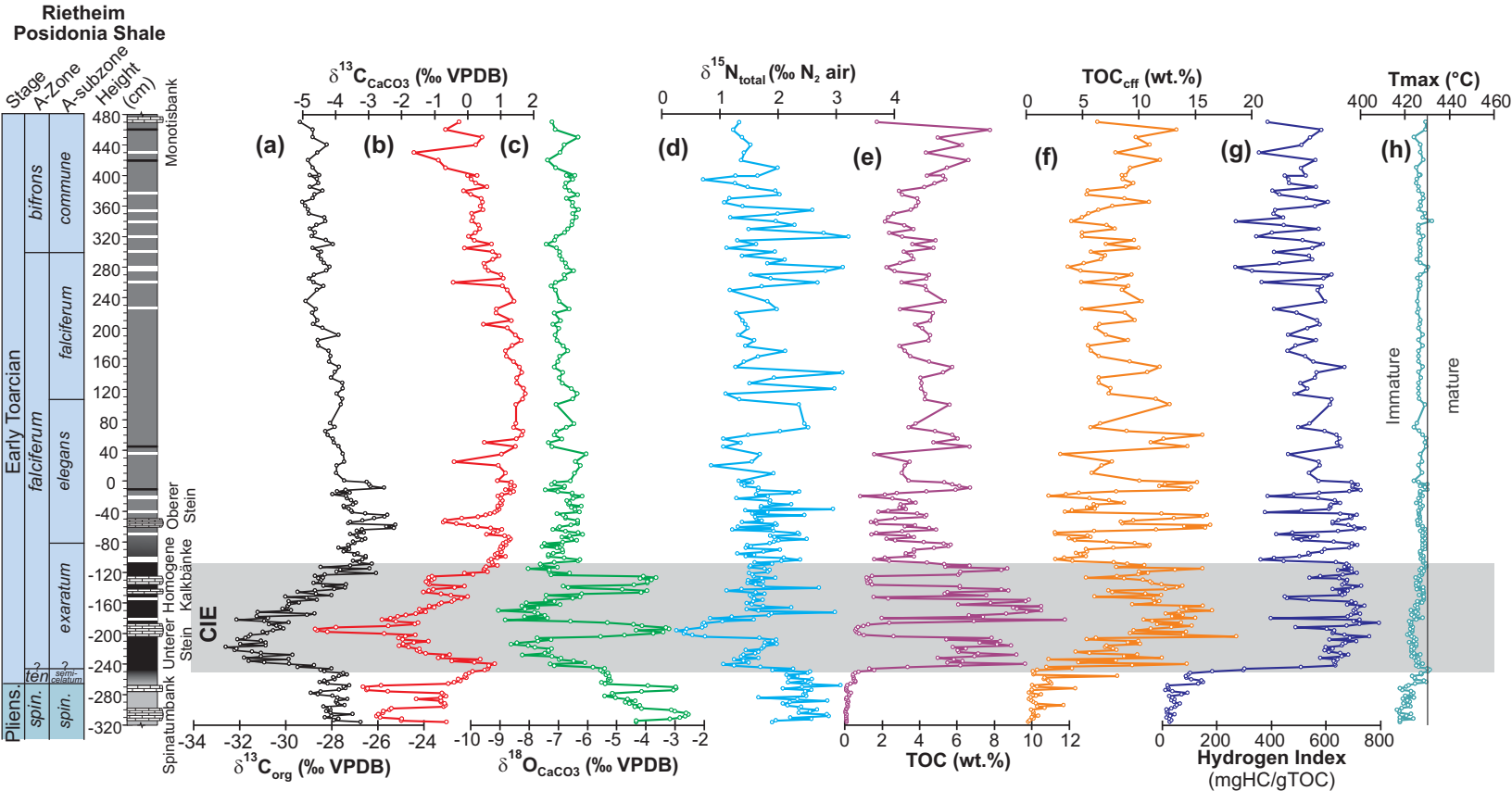

Figure 4

Figure 4

(single column)

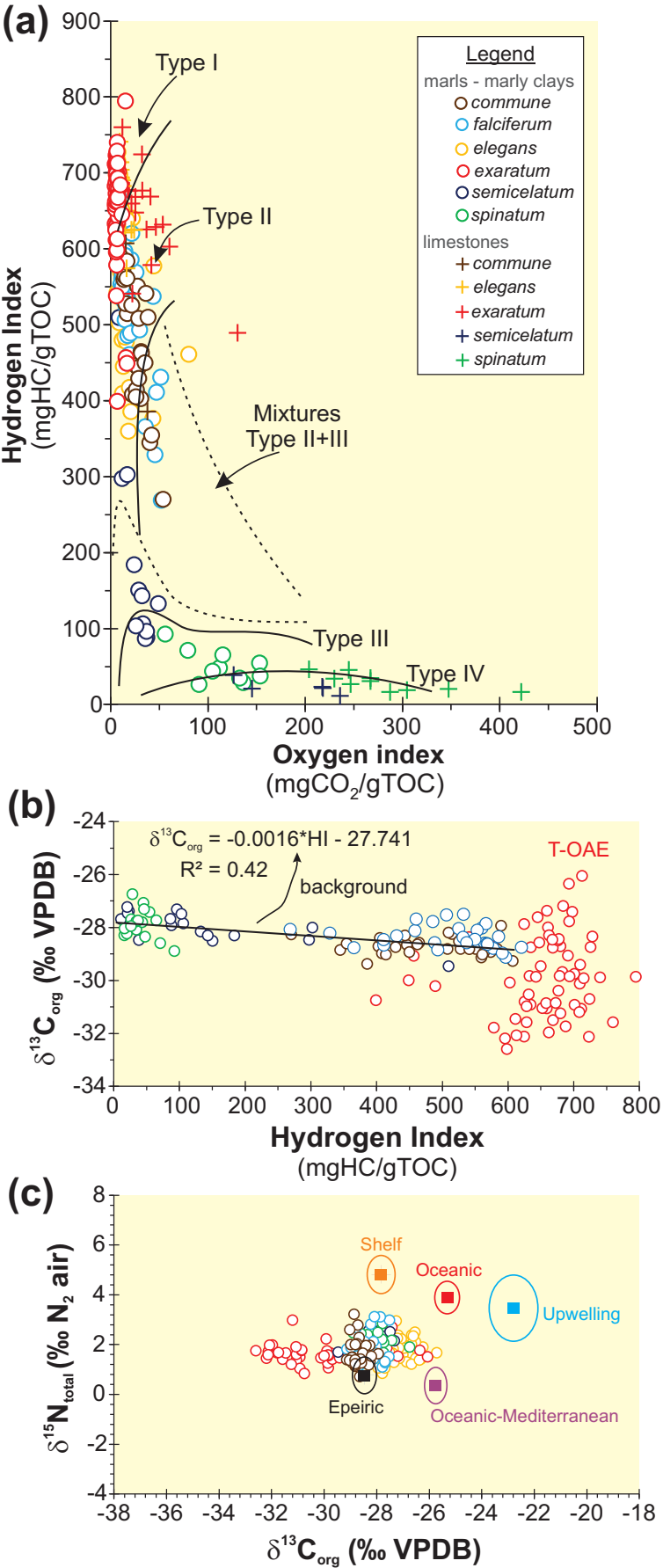

Figure 5

Figure 5

(single column)

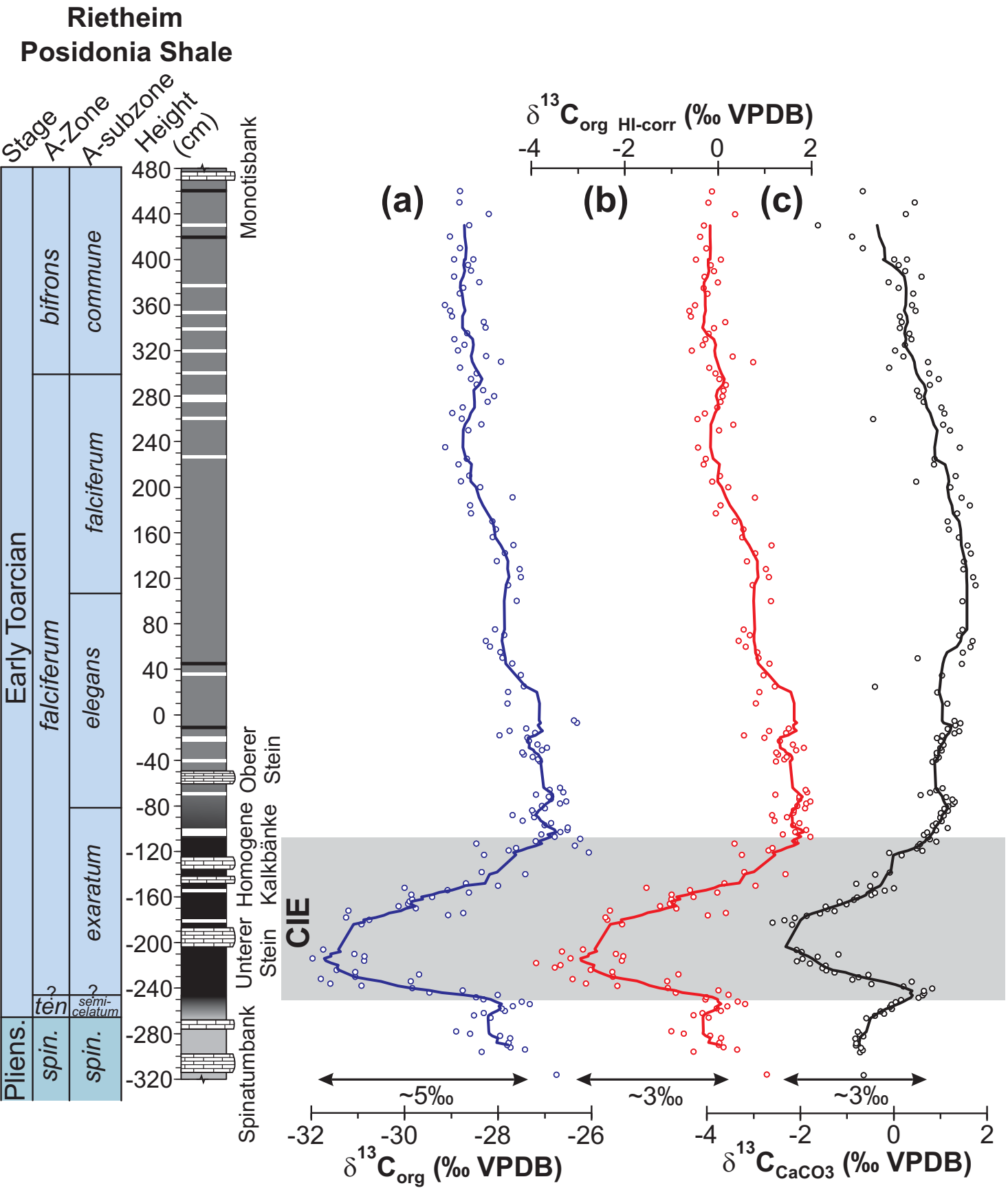

Figure 6

Figure 6

(Double column - full page width)

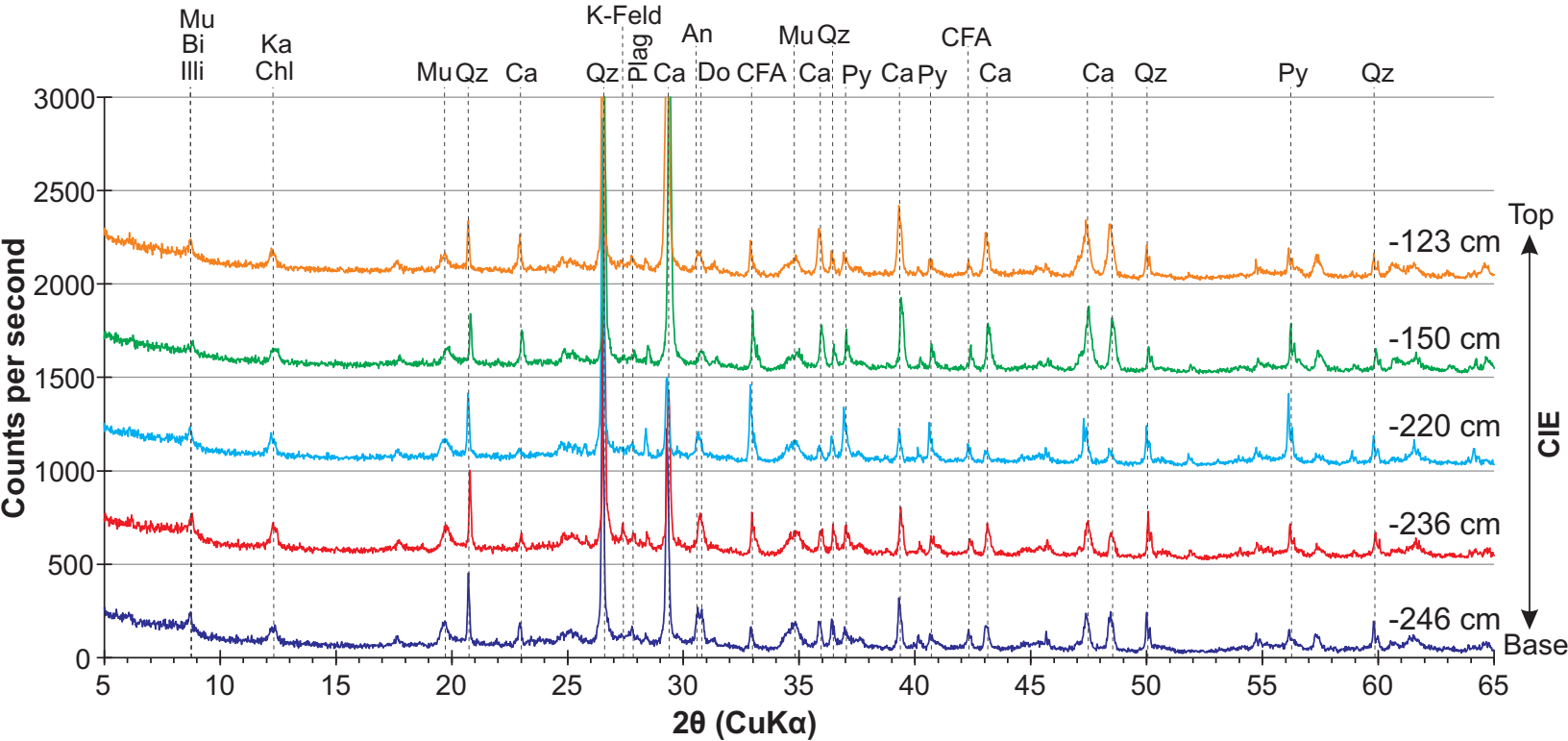

Figure 7

Figure 7

(Double column - full page width)

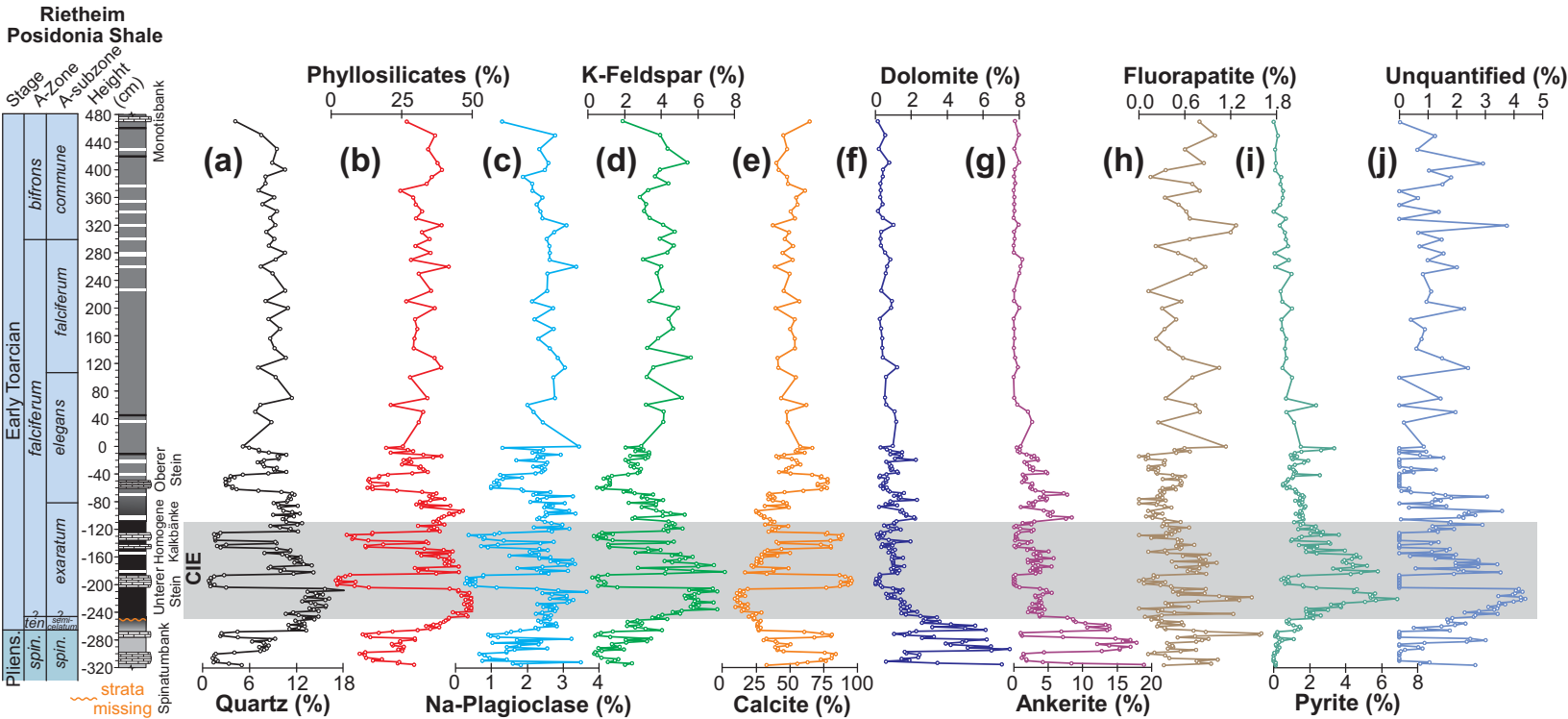

Figure 8

Figure 8

(Double column - full page width)

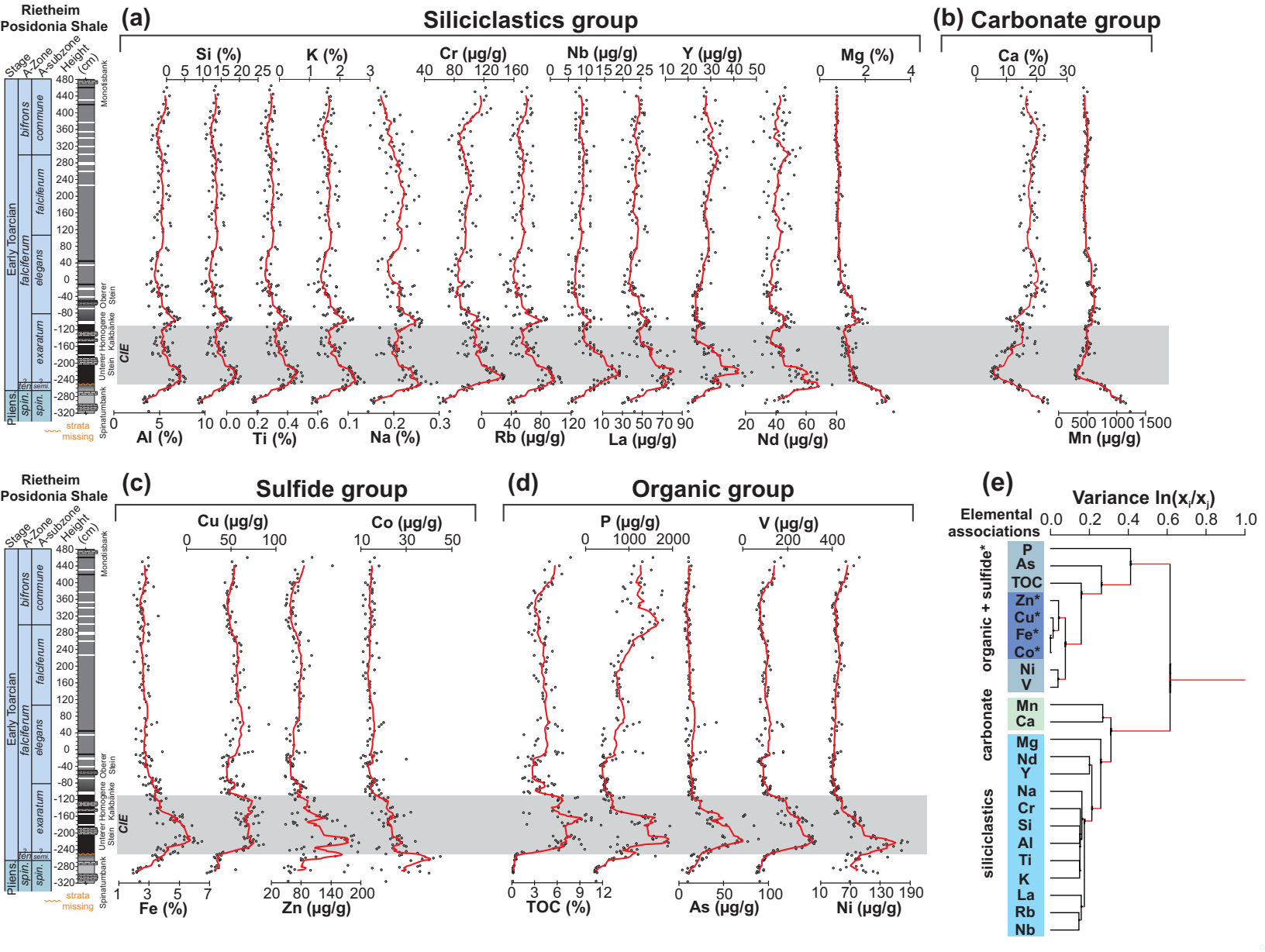

Figure 9

Figure 9

(Double column - full page width)

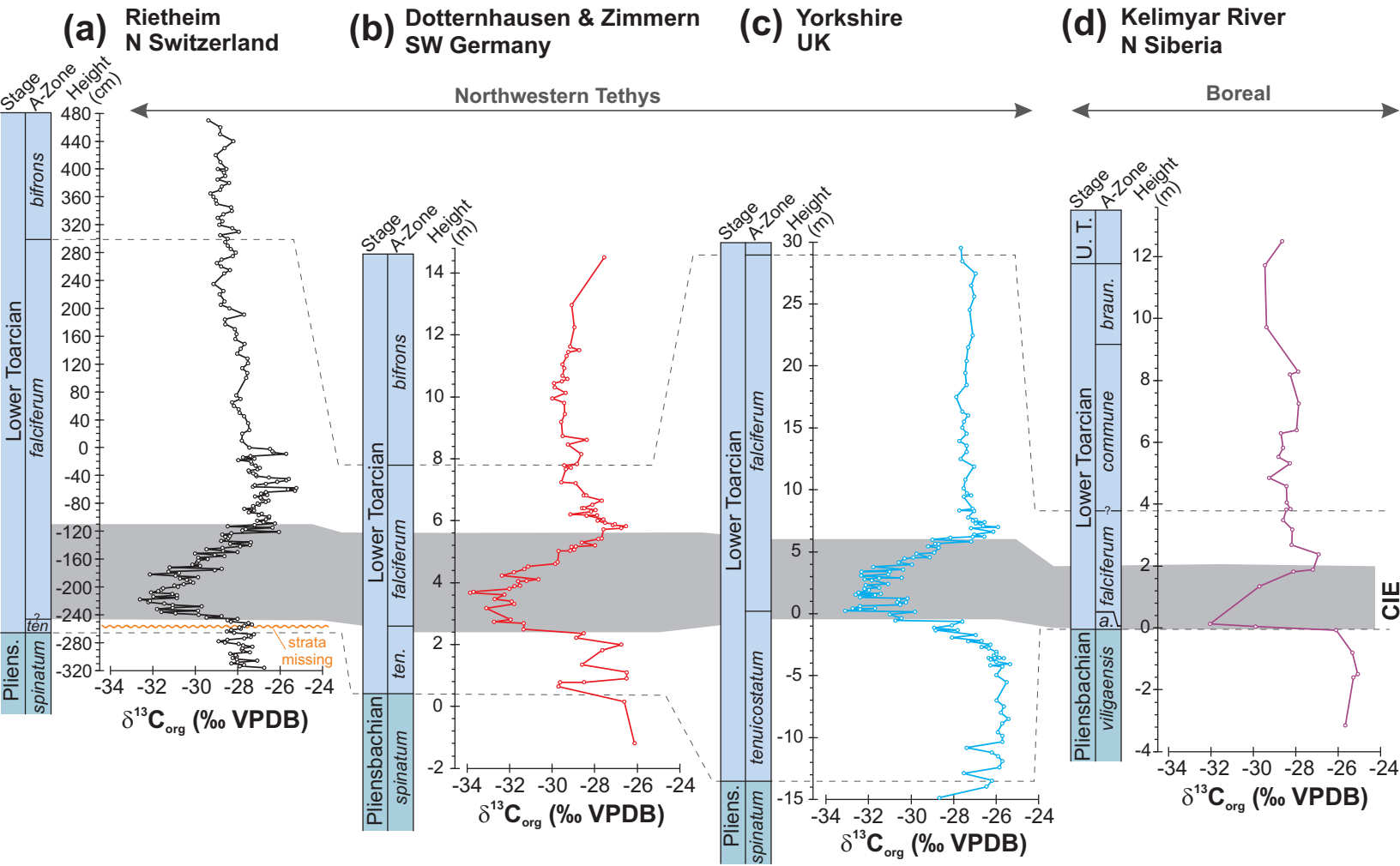

Figure 10

Figure 10

(single column)

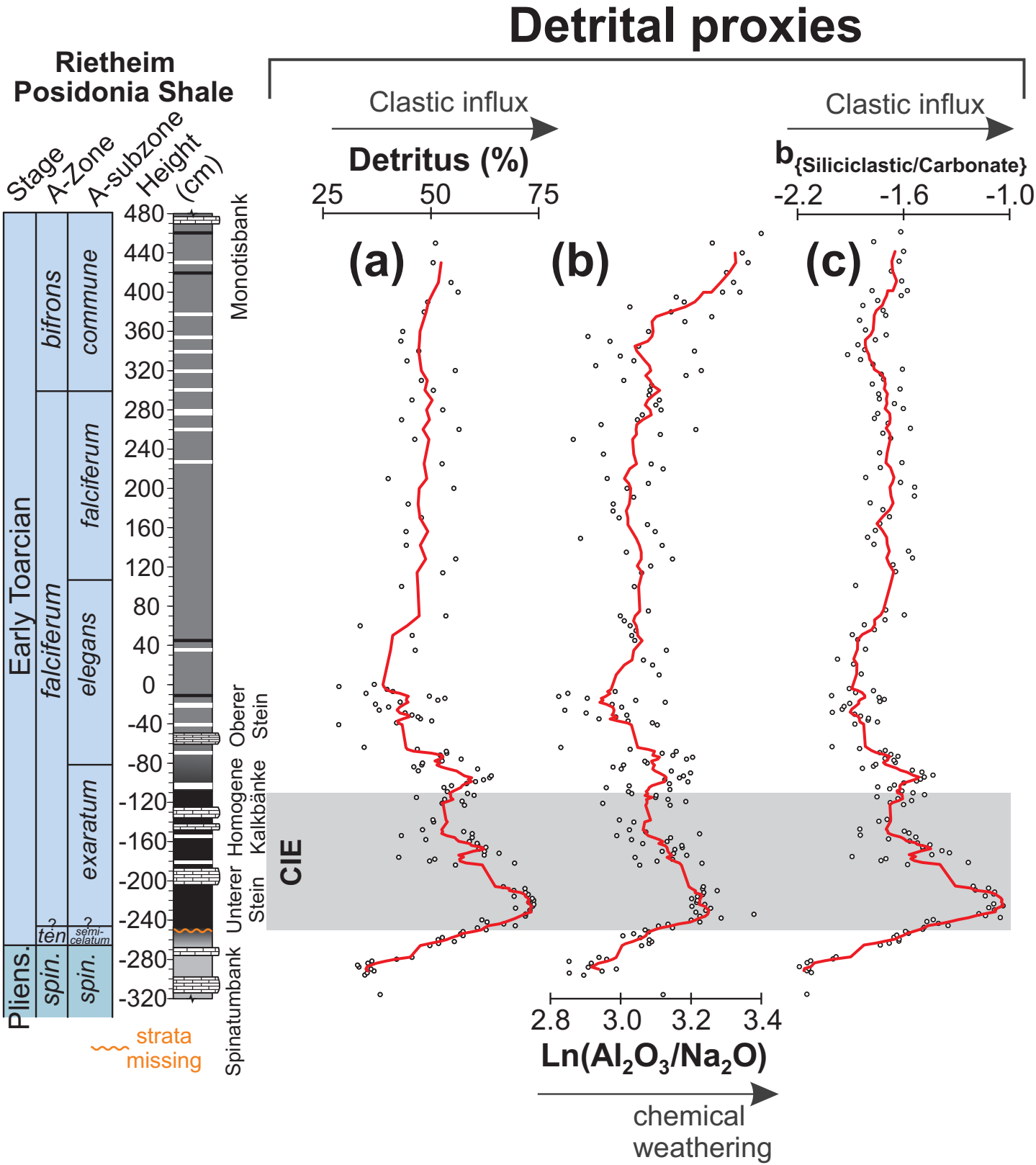

Figure 11

Figure 11

(Double column - full page width)

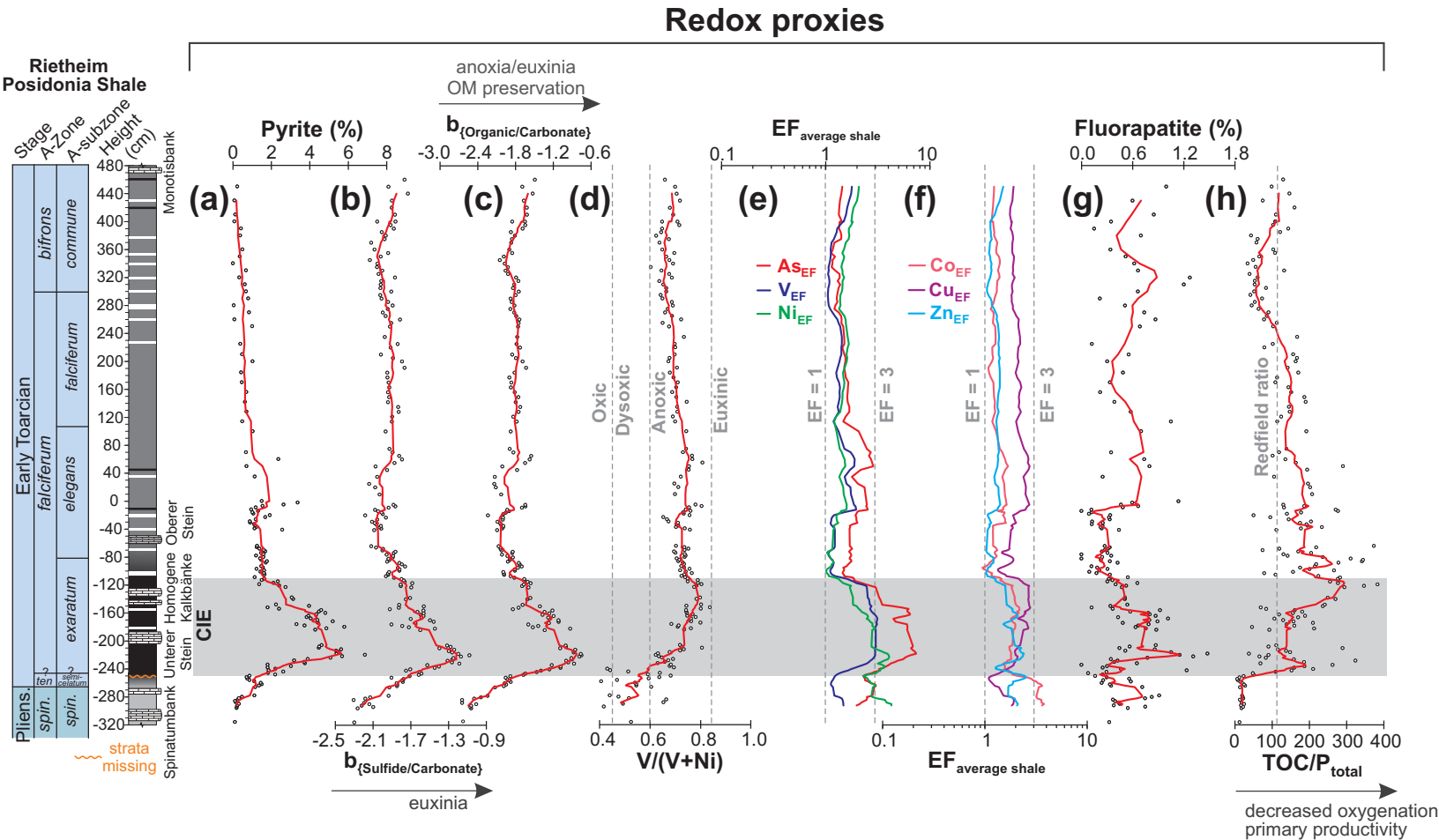

Figure 12

Figure 12

(single column)

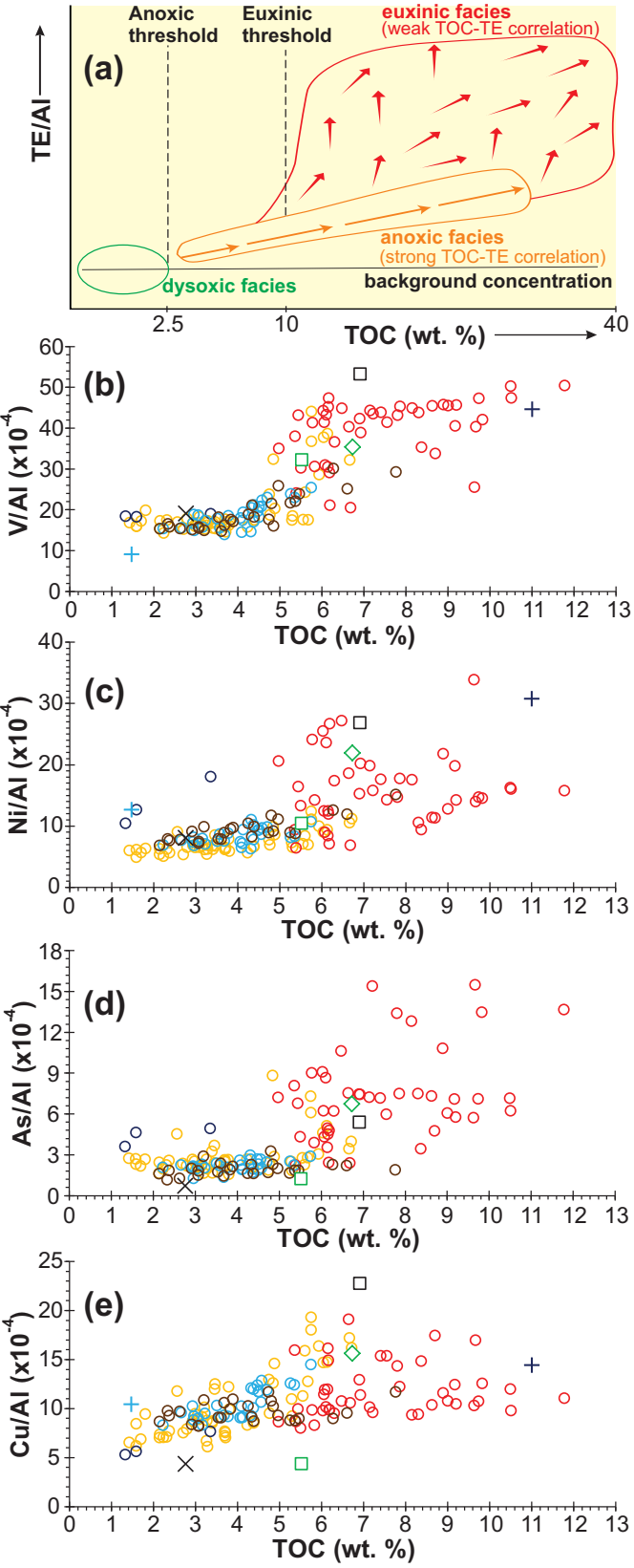

Legend

Redox facies

Posidonia Shale Rietheim
- *semicelatum* (Base)
- *exaratum*
- *elegans*
- *falciferum*
- *commune* (Top)

Posidonia Shale SW Germany
- Anoxic

Upper Pennsylvanian black shales
- Anoxic
- Dysoxic

Sapropels
- Anoxic - Euxinic

Cariaco Basin
- Anoxic

Southern California margin
- Dysoxic